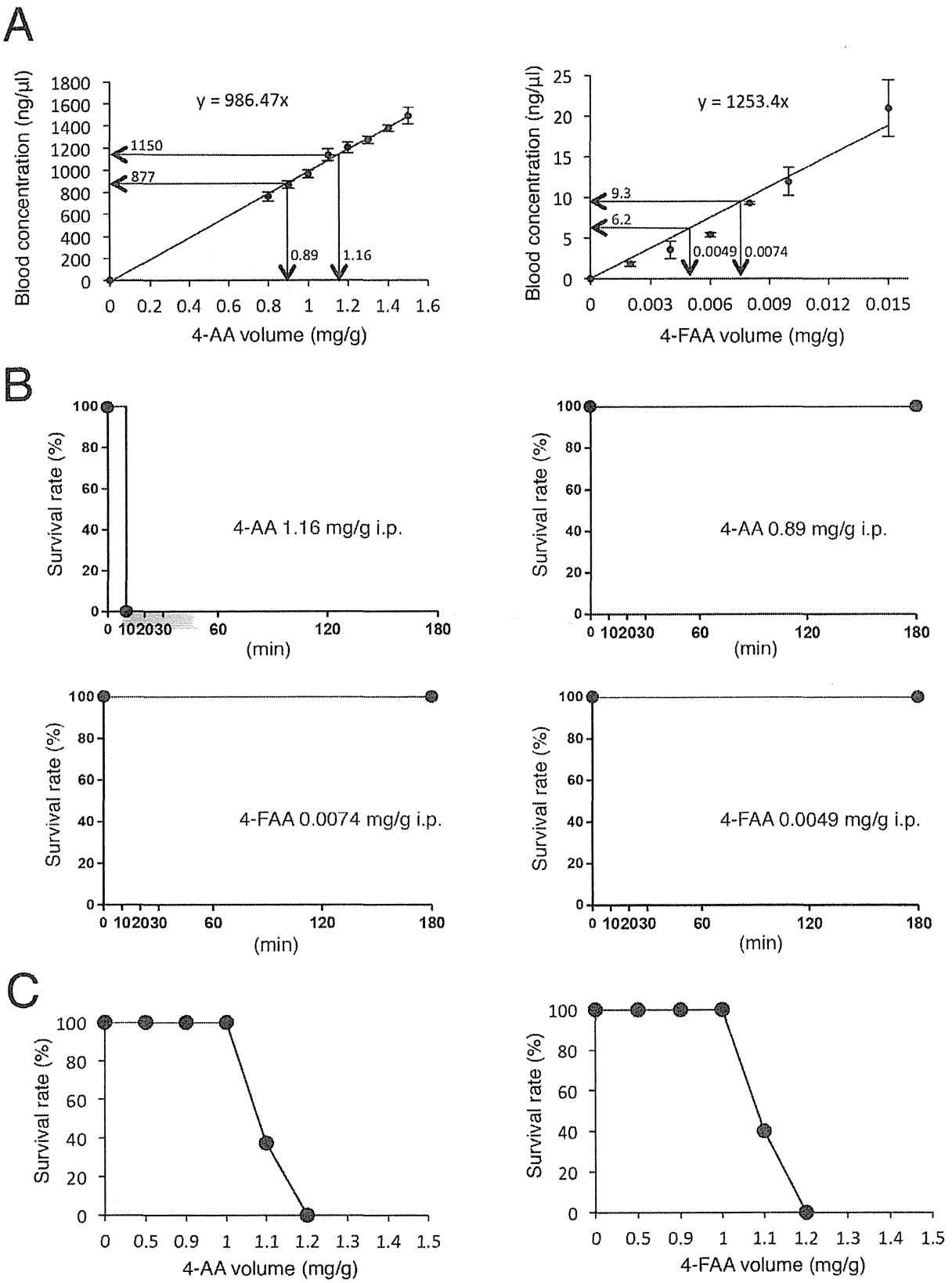

Figure 2. The blood concentration of 4-AA is involved in sulpyrine-induced shock. (A) Calibration curves for relationship between the administration volumes of 4-AA, 4-FAA and the concentrations of in the sera. (B) Wild-type mice (n = 5) were intraperitoneally injected with indicated volumes of 4-AA and 4-FAA. Survival rate was monitored for 180 min. (C) Wild-type mice (n = 5) were intraperitoneally injected with indicated volumes (0, 0.5, 0.9, 1.0, 1.2, 1.3, 1.4, and 1.5 mg/g) of 4-AA and 4-FAA. Survival rate was monitored for 180 min. Data are representative of two (A–C) independent experiments.
doi:10.1371/journal.pone.0055800.g002

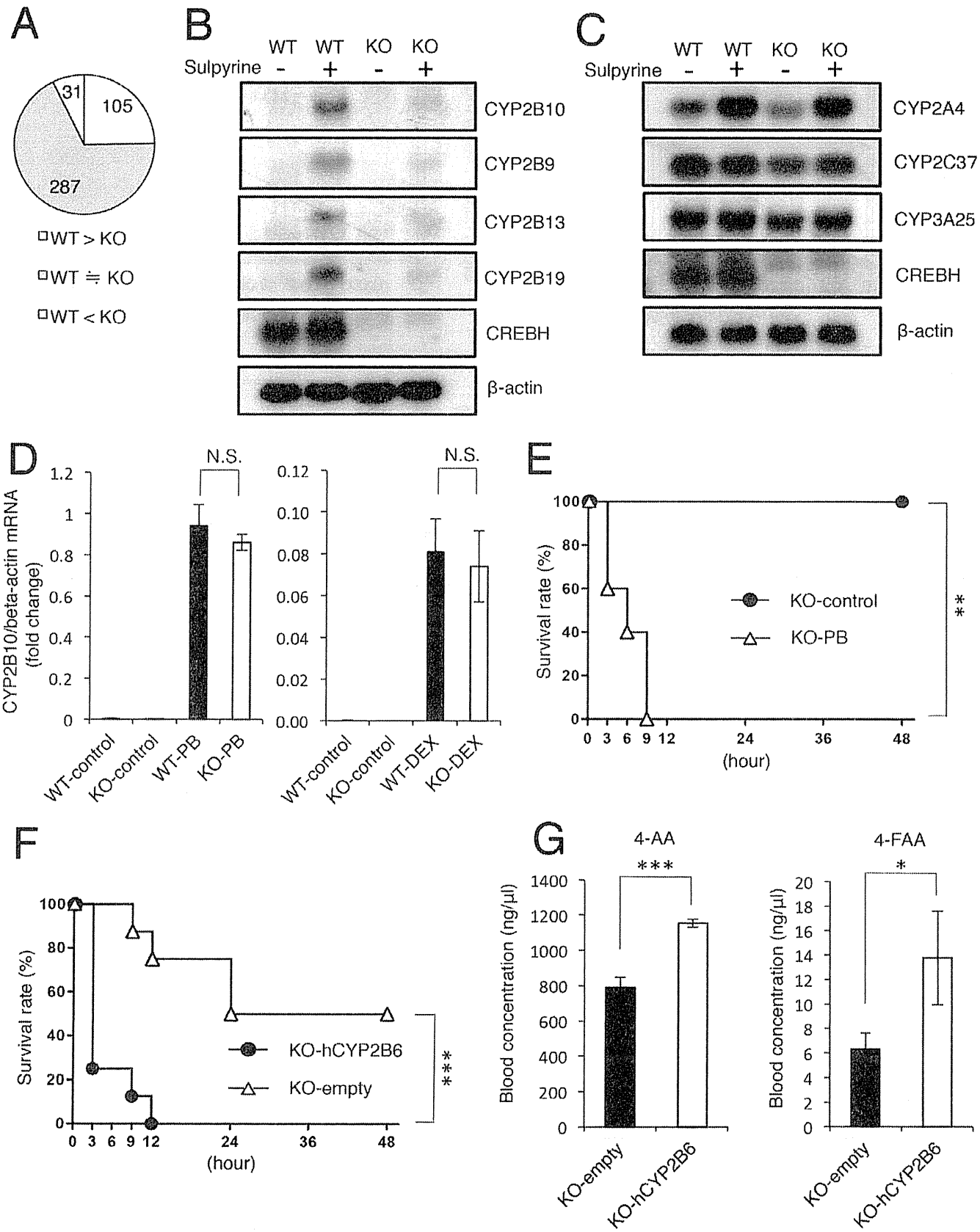

Figure 3. Sulpyrine-induced hepatic expression of CYP2B family genes is severely diminished in CREBH-deficient mice. (A) Summary of the microarray analysis. 423 sulpyrine-inducible genes were divided into down-regulated (yellow), similarly expressed (pink), and up-regulated (blue) groups, with the indicated amount of each. (B, C) Wild-type and CREBH-deficient mice were intraperitoneally injected with 2.7 mg/g of

sulpyrine or vehicle alone (control). At 24 hr after injection, livers were taken from these mice. Total RNA was extracted and subjected to northern blot analysis for expression of the indicated probes. The same membrane was rehybridized with a β-actin probe. (D) Wild-type mice and CREBH-deficient mice were intraperitoneally injected with 100 mg/kg phenobarbital (n = 3) or vehicle alone (control) (n = 3) every 24 hr for 3 days (left), or were intraperitoneally injected with 50 mg/kg dexamethasone (n = 7) or vehicle alone (control) (n = 3) (right). At 24 hr after the last injection, livers were taken from these mice. Gene expression of CYP2B10 was analysed by a quantitative RT-PCR assay. N.S., not significant. (E) CREBH-deficient mice were pre-treated with 100 mg/kg PB (n = 5) or vehicle alone (control) (n = 5) every 24 hr for 3 days. At 24 hr after the last injection, the mice were intraperitoneally injected with 1.1 mg/g of sulpyrine. Survival rate was monitored for 48 hr. (F) CREBH-deficient mice transfected with hCYP2B6 expression vectors (n = 8) or empty vectors (n = 8) were intraperitoneally injected with 2.7 mg/g of sulpyrine. Survival rate was monitored for 48 hr. (G) CREBH-deficient mice transfected with hCYP2B6 expression vectors (n = 3) or empty vectors (n = 3) were intraperitoneally injected with 2.7 mg/g of sulpyrine. Sera were taken at 2 hr 40 min after sulpyrine injection. Serum concentrations of 4-AA and 4-FAA were measured by a HPLC assay. *, $P<0.05$; ***, $P<0.001$. Data are pooled from two (E) independent experiments or representative of two (A, B, C, D, F) independent experiments.
doi:10.1371/journal.pone.0055800.g003

transfected the RNAi vector into wild-type mice *in vivo*, and confirmed the efficiency of *in vivo* knockdown in the liver by a quantitative RT-PCR assay (Figure 6A). Next, we administrated sulpyrine to CREBH-knockdown mice, and then measured the survival rate and blood concentrations of 4-AA and 4-FAA. CREBH-knockdown mice exhibited resistance to fatal sulpyrine shock, compared with that of control mice (Figure 6B). In addition, blood concentrations of 4-AA and 4-FAA in CREBH-knockdown mice were lower than those in control mice (Figure 6C). Thus, these results suggest that RNAi-mediated suppression of CREBH can alleviate fatal sulpyrine shock.

Discussion

It has been almost a century since sulpyrine became a widely-used therapeutic drug. Despite the severe side effects, sulpyrine is generally used both in the adults and children as a first-line antipyretic analgesic in some developed countries as well as a number of developing countries [32–35]. Severe shock is a fatal side effect of pyrazolone derivatives including sulpyrine. The peculiar symptoms such as loss of consciousness, coma, and convulsions are associated with the shock, eventually leading to a lethal condition or death in some patients [36,37]. In fact, severe convulsions were also observed in sulpyrine-administrated mice in our study (data not shown). Therefore, sufficient caution should be exercised in sulpyrine medication. However, pathogenic mechanism of sulpyrine-induced shock is poorly understood. In this study, we identify that 4-AA, one of the sulpyrine metabolites, is the causative substance of sulpyrine-induced shock. In addition to sulpyrine, another pyrazolone derivative, aminopyrine is metabolized to 4-AA [38], and cause anaphylactic shock as a side effect [39], suggesting that 4-AA may be the causative substance of the shock.

In this study, we demonstrate that CREBH mediates sulpyrine-induced fatal shock. Upon ER stress, CREBH is previously reported to translocate to the Golgi apparatus, and cleaved by S1P and S2P as well as SREBPs. The cleaved cytosolic lesion of the N-terminal CREBH traffics to the nucleus [12]. We show that CREBH was activated by sulpyrine-induced ER stress, and trafficked to the nucleus to activate transcriptional induction of CYP2B family genes in the liver. CYP2B induced by CREBH increased the serum concentration of 4-AA, which has the antipyretic effect. Furthermore, CREBH-deficient mice with ectopic expression of hCREBH or CYP2B6 became sensitive to sulpyrine, suggesting that CREBH or CYP2B was a critical trigger for the sulpyrine-induced fatal shock. CAR and PXR are known as the transcriptional activators of CYP2B family genes. Although, we originally hypothesized that CREBH was involved in the induction of CYP2B family genes collaborated with CAR or PXR, our data suggested that CREBH induced transcription of CYP2B family genes independently of either CAR or PXR.

APAP is a widely used antipyretic analgesic drug. It has been recently reported that hepatic XBP1-deficient mice were resistant to APAP-induced hepatic dysfunction due to low expression levels of mRNAs of CYP1A2 and CYP2E1, both of which are metabolic enzymes for APAP to produce NAPQI by hydroxylation of acetaminophen [16,40–42]. NAPQI is normally detoxified by glutathione conjugation. However, NAPQI is accumulated in the liver by the mass administration of APAP and the hepatic dysfunction, it binds to biopolymer which induces hepatic necrosis [43]. Although subclasses of CYP enzymes, which expression were reduced in the mutant mice were different (i.e. CYP2B or CYP1A2/CYP2E1 for CREBH or XBP1, respectively), mice deficient in ER stress related transcription factors showed resistance to the fatal side effect of antipyretic analgesic drugs because of the low CYP expression. However, the mechanism of the reduced CYP expression by the deficiency of each transcription factor is different. The XBP1 deficiency leads to upregulation of the ribonuclease IRE1α, which degrades mRNA for CYP1A2/CYP2E1, suggesting the indirect reduction of CYP1A2/CYP2E1 by the XBP1-deficiency [16]. On the other hand, CREBH directly induces CYP2B expression upon sulpyrine stimulation. The difference might be caused by the property or injected dose of these drugs. Furthermore, tunicamycin, which is known to activate CREBH, upregulated CYP2B10 strongly in the liver (Figure 4C). Thus, other hepatic ER stress inducible drugs might be able to induce CYP2B family genes via CREBH activation.

Recently, some NSAIDs have been reported to induce ER stress. Indomethacin treatment induces ER stress in murine podocytes [44], and CHOP expression in gastric mucosal cells of guinea pig, resulting in apoptosis [45]. The CHOP-mediated apoptosis is also stimulated by other NSAIDs such as celecoxib and sulindac sulfide, in human gastric cells and colon epithelial cancer cells, respectively [46] [47]. The gastric ulcer is the representative side effect in NSAIDs [48]. On the other hand, the incidence rate of cancer has been shown to lower by a long-term NSAIDs medication [49,50]. Although these molecular mechanisms remain unclear, the involvement of NSAIDs-induced ER stress in these phenomena is suggested [51,52]. Treatment of some NSAIDs such as indomethacin, diclofenac, etodolac, ibuorofen, celecoxib, and ketoprofen increase intracellular Ca^{2+} levels, and stimulate Ca^{2+} influx across the cytoplasmic membrane, leading to the increment of membrane permeability, mitochondrial dysfunction, and apoptosis [53]. Whether Ca^{2+} is also involved in sulpyrine-induced ER stress should be examined in the future.

In this study, we demonstrate that CREBH-dependent expression of CYP2B in the liver is one of the molecular mechanisms of fatal shock induced by sulpyrine in a mouse model. However, whether this mechanism also applies to humans remains unclear and it would be of interest to test whether the hepatic expression level of CREBH (and CYP2B) is relevant to sulpyrine-induced shock in humans. Furthermore, given that transient knockdown of CREBH prior to sulpyrine administration mitigates the shock in

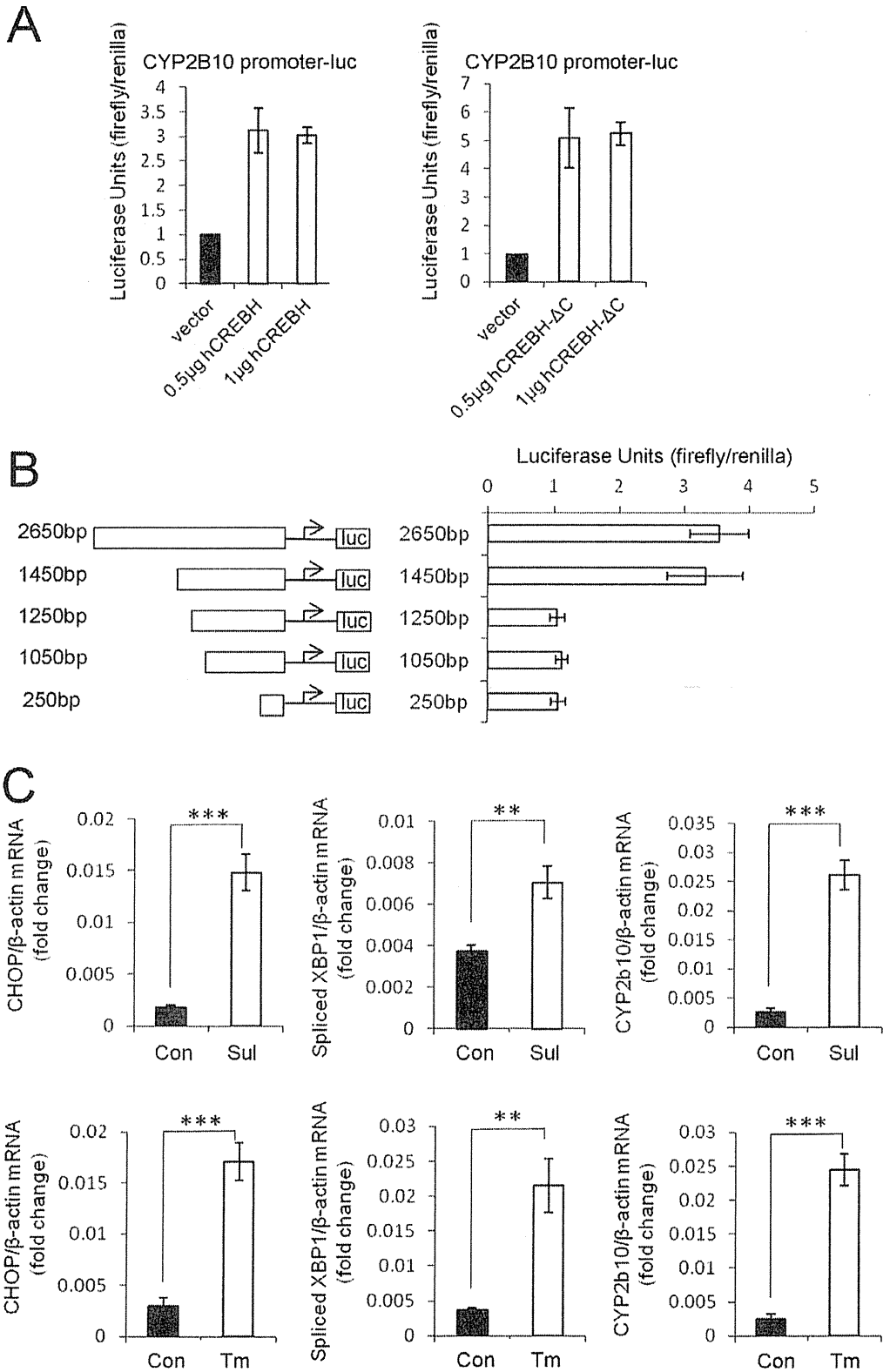

Figure 4. Sulpyrine treatment causes ER stress. (A) Huh7 cells were transiently transfected with luciferase reporter plasmids containing the CYP2B10 promoter together with control, hCREBH-F, or hCREBH-ΔC expression vector. Relative luciferase activities were shown as fold increases over the background levels shown by lysates prepared from control vector-transfected cells. Error bars are means ± S.D. of triplicates. (B) Huh7 cells were transiently transfected with luciferase reporter plasmids containing the indicated length CYP2B10 promoter together with control or hCREBH-F expression vector. Relative luciferase activities were shown as fold increases over the background levels shown by lysates prepared from control vector-transfected cells. Error bars are means ± S.D. of triplicates. (C) Wild-type mice were intraperitoneally injected with 2.7 mg/g of sulpyrine (n = 3) or 200 μg/kg tunicamycin (n = 3) or vehicle alone (control) (n = 3). At 2 hr 40 min after injection, hepatocytes were taken from these mice by a

perfusion apparatus. Gene expression of CHOP, spliced XBP1, and CYP2B10 was measured by a quantitative RT-PCR assay. **, P<0.01; ***, P<0.001. Data are representative of three (A, B) and two (C) independent experiments.
doi:10.1371/journal.pone.0055800.g004

mice, therapeutic application of a molecule that inhibits CREBH action might be beneficial for patients that are sensitive to sulpyrine.

Materials and Methods

Generation of CREBH-deficient mice

The CREBH gene was isolated from genomic DNA extracted from ES cells (V6.5) by PCR using TaKaRa LA Taq^{TM} (TaKaRa) [54]. The targeting vector was constructed by replacing a fragment encoding the exons of *CREBH* with a neomycin-resistance gene cassette (neo), and a herpes simplex virus thymidine kinase driven by PGK promoter was inserted into the genomic fragment for negative selection. A genomic DNA containing the murine *CREBH* gene was isolated from PCR amplification by using primer CREBHKO_LA_F and CREBH-KO_LA_R, to generate a 5.0 kb long fragment, and CREBH-KO_SA_F and CREBHKO_SA_R, to generate a 1.0 kb short fragment. The sequences of primers are listed in Table S2. After the targeting vector was transfected into ES cells, G418 and gancyclovir doubly resistant colonies were selected and screened by PCR and southern blotting using the probe indicated in Fig S1A. Homologous recombinants were micro-injected into C57BL/6 female mice, and heterozygous F1 progenies were intercrossed in order to obtain CREBH-deficient mice. CREBH-deficient mice and their wild-type littermates from these intercrosses were used for experiments. Male mice (8–11 weeks old; approximately 25 g weight) were used in the present study. All animal experiments were conducted with approval of the Animal

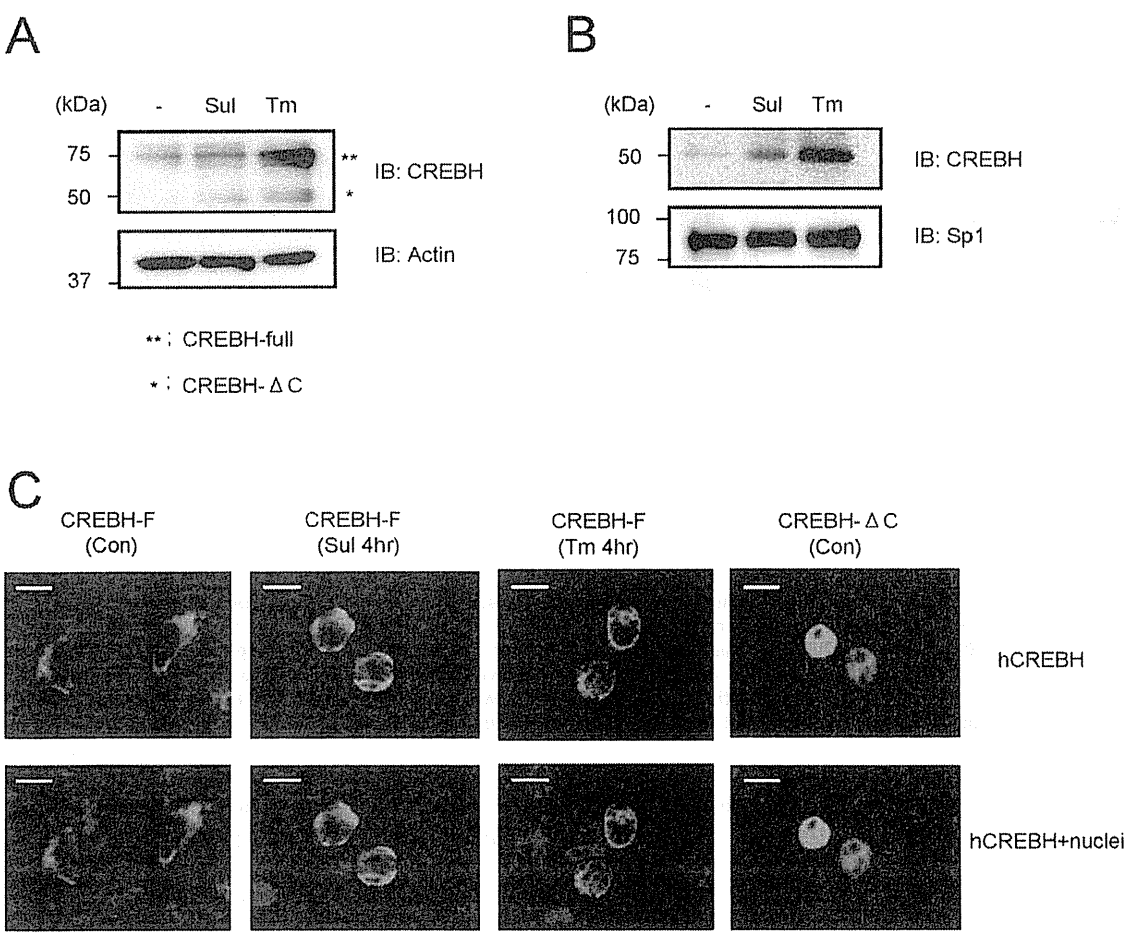

Figure 5. Cleavage of CREBH and its translocation into nucleus were induced by sulpyrine. (A) 293T cells were transiently transfected with 2 μg HA-tagged hCREBH-F expression vectors, and they were cultured with sulpyrine (2 mM) or tunicamycin (5 μg/ml) for 6 hr. Whole-cell lysates were prepared and the size of CREBH was analysed by western blot analysis using anti-CREBH monoclonal (upper panel) and anti-actin antibodies (lower panel). **, CREBH-full ; *, CREBH-ΔC. (B) 293T cells were transiently transfected with 2 μg HA-tagged hCREBH-F expression vectors, and they were cultured with sulpyrine (2 mM) or tunicamycin (5 μg/ml) for 6 hr. The cell lysates of nuclear fractions were prepared. The nuclear translocation of CREBH was analyzed by western blot analysis using anti-CREBH monoclonal (upper panel) and anti-Sp1 monoclonal antibodies (lower panel). (C) 293T cells were transiently transfected with HA-tagged hCREBH-F expression vectors and HA-tagged hCREBH-ΔC expression vectors, and they were cultured with mock, sulpyrine (2 mM) and tunicamycin (5 μg/ml) for 4 hr. Cells were stained with anti-HA mouse antibody, then stained with Alexa Fluor 594-conjugated anti-mouse IgG (red) together with DAPI (blue). Stained cells were analysed using a confocal microscope. Bars, 10 μm. Data are representative of three (A) and two (B,C) independent experiments.
doi:10.1371/journal.pone.0055800.g005

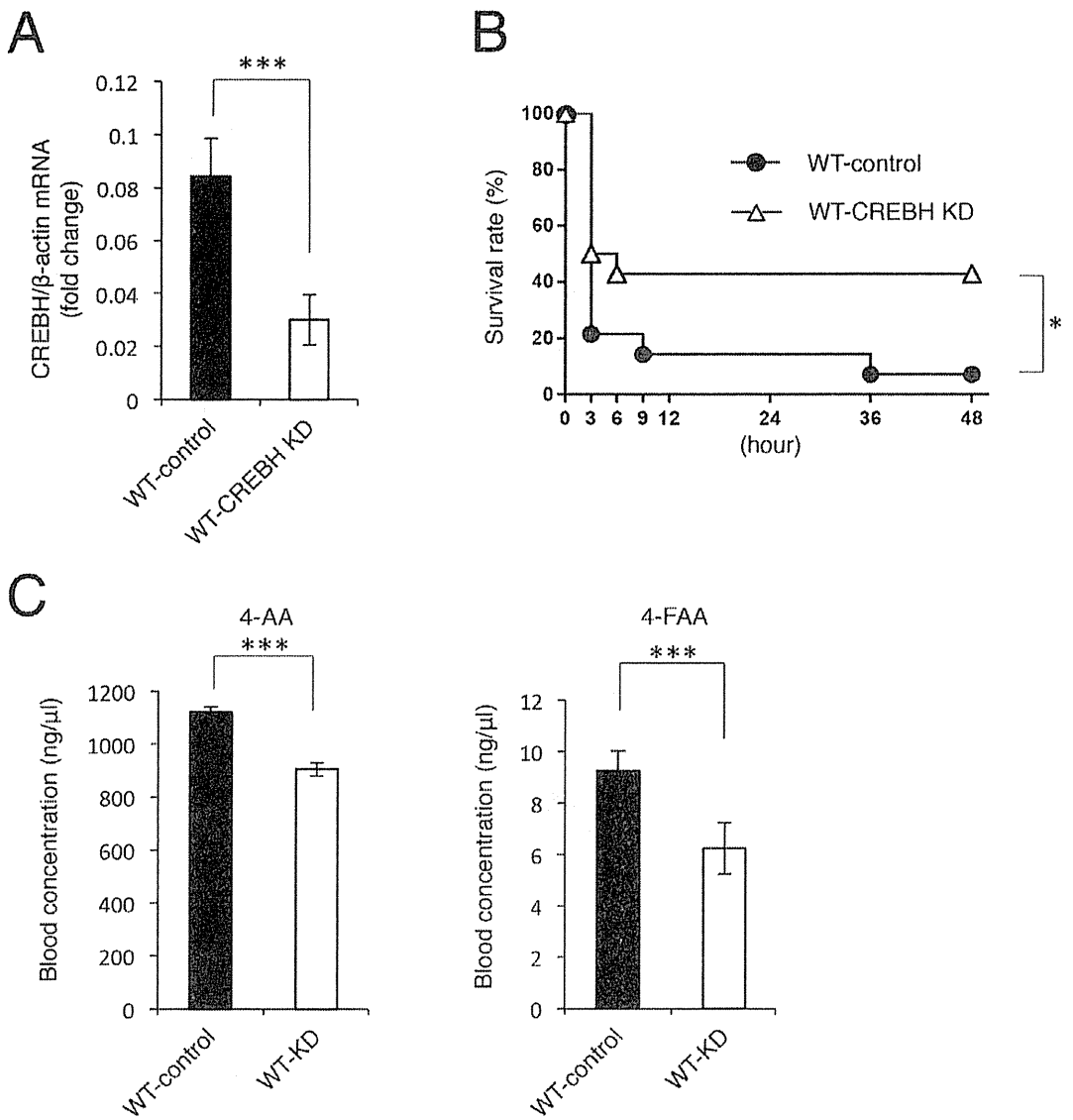

Figure 6. RNAi-mediated CREBH-knockdown mice are resistant to the sulpyrine shock. (A) Livers of wild-type mice transfected with RNAi vectors for CREBH (n = 4) or negative control vectors (n = 4) were taken at 24 hr after transfection. Gene expression of CREBH was analysed by a quantitative RT-PCR assay. ***, $P<0.001$. (B, C) Wild-type mice transfected with RNAi vectors for CREBH (n = 14) or negative control vectors (n = 14) were intraperitoneally injected with 2.7 mg/g of sulpyrine at 24 hr after transfection. Survival rate was monitored for 48 hr. *, $P<0.05$. Sera were taken at 2 hr 40 min after sulpyrine injection. Serum concentrations of 4-AA and 4-FAA were measured by a HPLC assay. ***, $P<0.001$. Data are representative of two (A, C) independent experiments or pooled from three (B) independent experiments.
doi:10.1371/journal.pone.0055800.g006

Research Committee of the Graduate School of Medicine at Osaka University.

Reagents

Sulpyrine Monohydrate, Phenobarbital Sodium were purchased from Wako. Dexamethasone was purchased from SIGMA. 4-Aminoantipyrine was purchased from nacalai tesque. 4-Formylaminoantipyrine was purchased from Aldorich Chemistry. Tunicamycin was purchased from Enzo Life Science. Anti-HA HRP, anti-actin HRP, anti-CREBH goat polyclonal immunoglobulin G, anti-goat immunoglobulin G HRP, anti-Sp1 rabbit polyclonal immunoglobulin G were purchased from Santa cruz. Alexa Fluor 488-conjugated anti-mouse immunoglobulin G, Alexa Fluor 594-conjugated anti-mouse immunoglobulin G, anti-rabbit immunoglobulin G HRP were purchased from Invitrogen. 4, 6-diamidino-2-phenylindole (DAPI) was purchased from Wako.

High performance liquid chromatography

HPLC equipment, consisting of Nanospace SI-2/3201 pump (SHISEIDO), Nanospace SI-2/3023 autosampler (SHISEIDO), Nanospace SI-2/3010 degasser (SHISEIDO), and Accela PDA Detector (Thermo Scientific) was used. A detector was operated at 254 nm wavelength. Separation was achieved with an μBondapak^{TM} C18 10 μm 125 A 3.9×150 mm column (Waters). The following eluent were used: 8% methanol in 0.01 M sodium acetate, adjusted to pH 3.0 with concentrated hydrochloric acid [55]. The column was maintained at room temperature and the flow-rate was 1000 μl/min. Serum samples were directly injected into the system after simple filtration with a membrane filter.

Aliquots of 4-AA and 4-FAA stock solution were diluted in the eluent and analyzed with the HPLC to obtain a standard curve. We compared the difference of the area under the curve of the sera with stock solution.

RNA interference

293T cells were cotransfected with 2 μg or 1 μg RNAi vectors targeting mouse CREBH in BLOCK-iT Pol II miR RNAi Expression Vector Kit (Invitrogen) and HA-tagged mCREBH expression vector. 24 hr after transfection, whole-cell lysates were prepared and subjected to Western blot analysis.

In vivo transfections

Twenty micrograms of expression plasmids for hCREBH or hCYP2B6, or RNAi vectors for mCREBH were mixed with 30 μl Lipofectamine 2000 reagent (Invitrogen) in 170 μl of Phosphate buffered saline (PBS), and the complexes were injected intravenously via orbital sinus [56].

Expression plasmids

Human CREBH cDNA was amplified using primers hCREBH_full_R for Full, hCREBH_ΔC_R for ΔC, and the common primer hCREBH_common_F using human liver cDNA as the template and then ligated into the *EcoRI* and *NotI* sites of a pcDNA vector for the N-terminal HA-tagged proteins (Invitrogen). Human CYP2B6 cDNA was amplified using primers CYP2B6_F and CYP2B6_R using human liver cDNA as the template and then ligated into the *BamHI* and *NotI* sites of a pcDNA vector for the N-terminal HA-tagged proteins. Human CAR cDNA was amplified using primers CAR_F and CAR_R using human liver cDNA as the template and then ligated into the *EcoRI* and *NotI* sites of a pcDNA vector for the N-terminal HA-tagged proteins. Murine CREBH cDNA was amplified using primers mCREBH_F and mCREBH_R using murine liver cDNA as the template and then ligated into the and *BglII* and *NotI* sites of a pcDNA vector for the N-terminal HA-tagged proteins. The sequences of primers are listed in Table S2.

Real-time RT-PCR

Total RNA of livers and hepatocyte were isolated with TRIzol reagent (Invitrogen), cDNA was generated using 5 μg of RNA and Verso cDNA Kit (Thermo Scientific). Real-time RT-PCR was performed on an ABI 7300 real-time PCR system (Applied Biosystems) using GoTaq qPCR Master Mix (Promega). All data were normalized to the β-actin expression, and the fold difference relative to the β-actin was shown. Amplification conditions were: 50°C (2 min), 95°C (10 min), 40 cycles of 95°C (15 s), and 60°C (60 s). Primers of hCREBH, mCREBH, CYP2B6, CYP2B10, CHOP, spliced XBP1 and β-actin were purchased from Invitrogen. The sequences of primers are listed in Table S2.

Immunohistochemical assay

Wild-type mice were transfected with HA-tagged pcDNA-CREBH or CYP2B6 expression vectors *in vivo*. At 24 hr after transfection, livers were taken and fixed with 4% paraformaldehyde (Wako) and cryoprotected in 10% sucrose for 10 min and 20% sucrose for 10 min, and embedded in OCT compound (SAKURA). 8 μm in thickness of liver cryostat sections were fixed in acetone, and washed with PBS. Sections were incubated with anti-HA (1:100) in Tris-HCl buffer saline (TBS) containing 1% bovine serum albumin, then incubated with Alexa Fluor 488-conjugated anti-mouse immunoglobulin G (1:100). To stain the nucleus, sections were cultured with DAPI (1:10000). The stained sections were mounted with Mountant, PermaFluor (Thermo SCIENTIFIC) and analyzed using a fluorescence microscope (FV1000-D IX81; Olympus).

Microarray analysis

Total RNA of livers were isolated with TRIzol reagent (Invitrogen), RNA quality was assessed with an Agilent Bioanalyser 2100 and only RNA with minimal degradation and distinct 18S and 28S rRNA bands were used for analysis. Fragmented and biotin-labeled cDNA was synthesized from 100 ng purified mRNA with GeneChip 3′IVT Express Kit Assay (Affymetrix). The cDNA was hybridized to Mouse Genome 430A 2.0 Array (Affymetrix). Hybridized chips were stained and washed and were scanned with GeneChip Scanner 3000 (Affymetrix). Genespring software (Silicon Genetics) was used for data analysis.

Northern blot analysis

Total hepatic RNA was extracted using the TRIzol reagent (Invitrogen). Fifteen μg of total RNA was electrophoresed, transferred to a nylon membrane, and hybridized with cDNA probes as described previously [57]. cDNA probes specific for CREBH, β-actin, CYP2B10, CYP2B9, CYP2B13, CYP2B19, CYP2A4, CYP2C37, and CYP3A25 were obtained by PCR with a set of specific primers from a mouse liver cDNA. The sequences of primers are listed in Table S2.

Luciferase reporter assay

The Luciferase reporter plasmids were transiently cotransfected into Huh7 cells with the control Renilla luciferase expression vectors using Lipofectamine 2000 reagent (Invitrogen). Luciferase activities of total cell lysates were measured using the Dual-Luciferase Reporter Assay System (Promega). The CYP2B10 promoter was amplified using primers CYP2B10 promoter_F for 1450 bp, CYP2B10 promoter_F for 1250 bp, CYP2B10 promoter_F for 1050 bp, CYP2B10 promoter_F for 250 bp, and CYP2B10 promoter_common_R using murine genomic DNA as the template. Luciferase reporter was generated by *MluI* fragment of the insertion the CYP2B10 promoter into the *MluI* site of pGL3 luciferase reporter. Luciferase reporter harboring CYP2B10 promoter for 2650 bp was generated by inserting the *MluI* fragment of the CYP2B10 promoter for 2650 bp into the *MluI* site of luciferase reporter harboring CYP2B10 promoter for 1450 bp. The CYP2B10 promoter for 2650 bp was amplified using primers CYP2B10 promoter_F for 2650 bp and CYP2B10 promoter_R for 2650 bp using murine genomic DNA as the template. The sequences of primers are listed in Table S2.

Preparation of primary mouse hepatocytes

Mice were anaesthetized, and subsequently the abdomen was opened to expose the liver. The perfusion needle (26 G TERUMO) was inserted into the portal vein, and the perfusion was started with 50 ml 37°C SC-1 solution consisting of 8000 mg/l NaCl, 400 mg/l KCl, 88.7 mg/l NaH2PO4·H2O, 120.45 mg/l Na2HPO4, 2380 mg/l HEPES, 350 mg/l NaHCO3, 190 mg/l EGTA, and 900 mg/l glucose (pH 7.25). When the perfusion was started immediately after cutting the ventral aorta. After all of SC-1 solution was flowed, the perfusion was continued to 100 ml 37°C SC-2 solution consisting of 8000 mg/l NaCl, 400 mg/l KCl, 88.7 mg/l NaH2PO4·H2O, 120.45 mg/l Na2HPO4, 2380 mg/l HEPES, 350 mg/l NaHCO3, and 560 mg/l CaCl2·2H2O (pH 7.25) added 0.2 μg/ml collagenase D from *Clostridium histolyticum* (Roche) and 0.02 μg/ml trypsin inhibitor from chicken egg white (SIGMA). After all of SC-2 buffer was flowed, steeped

the liver to SC-2 buffer, and breached a hepatic capsule, and shaken gently on ice. The liver was crumbled gently with an autopipetter, and filtered with a gauze. The hepatocytes were separated by low speed centrifugation (400 r.p.m.), and the obtained pellets were washed with ice-cold SC-2 buffer to purify the cells [58].

Immunofluorescence analysis

293T cells were transfected with 2 μg HA-tagged hCREBH expression vectors by Lipofectamine 2000 reagent (Invitrogen). After 24 hr, the cells were stimulated with 2 mM sulpyrine or 5 μg/ml Tunicamycin for 4 hr, and washed with PBS, and then fixed with 4% paraformaldehyde (Wako) for 10 min at room temperature. After 15 min permeabilization with 0.2% Triton X-100, cells were washed with PBS, and blocked with Blocking One (nacalai tesque) for 10 min, and incubated with anti-HA (1:100) in TBS containing 1% bovine serum albumin, then incubated with Alexa Fluor 594-conjugated anti-mouse immunoglobulin G (1:100). To stain the nucleus, cells were cultured with DAPI (1:10000). The stained cells were mounted with ProLong Gold antifade reagent (Invitrogen) on glass slides and analyzed using a fluorescence microscope (FV1000-D IX81; Olympus).

Western blot analysis

293T cells were lysis buffer containing 1% Nonidet P-40, 150 mM NaCl, 20 mM Tris-HCl, 1 mM EDTA, pH 7.5, and protease inhibitor cocktail (Roche). The cell lysates were separated by SDS-PAGE and transferred to PVDF membranes, and subjected to Western blot analysis using the indicated antibodies as described previously [59].

Isolation of nuclear fractions

Cells were treated with indicated stimulants. Treated cells were washed with PBS, lysed by Buffer A (10 mM HEPES-KOH (pH 7.8), 10 mM KCl, 0.1 mM EDTA (pH 8.0), 0.1% Nonidet P-40) and incubated on ice for 5 min. Lysates were centrifuged at 5000 r.p.m. for 5 min, then the pellets were re-suspended by Buffer C (50 mM HEPES-KOH (pH 7.8), 420 mM KCl, 0.1 mM EDTA (pH 8.0), 5 mM $MgCl_2$, 20% Glycerol) and protease inhibitor cocktail (Roche) and incubated on ice for 30 min. To isolate nuclear fractions, lysates were centrifuged at 14000 r.p.m. for 10 min. The resulting supernatants contained the nuclear fractions.

Statistical analysis

We used unpaired student's t-test and log-rank test to determine statistical significance among experimental data.

Supporting Information

Figure S1 Targeted disruption of the murine *CREBH* gene. (A) The structure of the murine *CREBH* gene, the targeting vector and the predicted disrupted gene. Open boxes denote the coding exon. H, *HincII*; B, *BamHI*. (B) Southern blot analysis of offspring from the heterozygote intercrosses. Genomic DNA was extracted from mouse tails, digested with *HincII* and *BamHI*, separated by electrophoresis and hybridized with the radiolabelled probe indicated in (A). Southern blotting gave a single 2.5-kb band for wild-type (+/+), a 1.7-kb band for homozygous (−/−) and both bands for heterozygous (+/−) mice. (C) Northern blot analysis of liver cells taken from wild-type and CREBH-deficient mice. Total RNA (15 μg) extracted from livers was separated by electrophoresis, transferred to nylon membrane and hybridized using the CREBH fragment as a probe. The same membrane was rehybridized with a β-actin probe.
(TIF)

Figure S2 Illustration of the metabolite of sulpyrine. Sulpyrine is non-enzymatically hydrolysed to 4-methylaminoantipyrine (4-MAA), which is further metabolized to 4-aminoantipyrine (4-AA), and 4-formylaminoantipyrine (4-FAA) in the liver.
(TIF)

Figure S3 HPLC chromatograms for the identification of 4-AA and 4-FAA. (A) Representative HPLC chromatograms of 4-AA standard (left) and 4-FAA standard (right). (B) A representative HPLC chromatogram of serum sample of sulpyrine-administrated mouse. Data are representative of three (A, B) independent experiments.
(TIF)

Figure S4 Almost 1000 ng/ul 4-AA in the sera is the threshold of live-and-dead. (A) Wild-type mice were intraperitoneally injected with 1.1 mg/g of 4-AA. Sera of alive group (n = 4) and dead group (n = 5) were taken at indicated time points. Serum concentration of 4-AA were measured by a HPLC assay. The assay was performed on mice only when they were alive. N.D., not detected. ***, $P<0.001$. (B) Wild-type (n = 5) and CREBH-deficient (n = 5) mice were intraperitoneally injected with 1.1 mg/g of 4-AA and 4-FAA. Survival rates were monitored for 180 min and 48 hr. Data are representative of two (A, B) independent experiments.
(TIF)

Figure S5 *In vivo* transfection of human CREBH. (A, B) CREBH-deficient mice were transfected with HA-tagged hCREBH expression vectors (n = 4) or empty vectors (n = 4). At 24 hr after transfection, livers were taken from these mice. Gene expression of hCREBH was analysed by a quantitative RT-PCR and an Immunofluorescence assay. The sections were stained with anti-HA mouse antibody, then stained with Alexa Fluor 488-conjugated anti-mouse IgG (green) together with DAPI (blue). Stained cells were analysed using a confocal microscope. Bars, 100 μm. ***, $P<0.001$. Data are representative of two (A, B) independent experiments.
(TIF)

Figure S6 *In vivo* transfection of human CYP2B6. (A, B) CREBH-deficient mice were transfected with HA-tagged hCYP2B6 expression vectors (n = 4) or empty vectors (n = 4). At 24 hr after transfection, livers were taken from these mice. Gene expression of hCYP2B6 was analysed by a quantitative RT-PCR and an Immunofluorescence assay. The sections were stained with anti-HA mouse antibody, then stained with Alexa Fluor 488-conjugated anti-mouse IgG (green) together with DAPI (blue). Stained cells were analysed using a confocal microscope. Bars, 100 μm. ***, $P<0.001$. Data are representative of two (A, B) independent experiments.
(TIF)

Figure S7 CREBH and CAR independently activate CYP2B10 promoter. (A) Illustration of luciferase reporter plasmids containing the CYP2B10 promoter with or without the CAR responsive element called Nr1 region. (B) Huh7 cells were transiently transfected with luciferase reporter plasmids containing the CYP2B10 promoter with or without Nr1 region together with control or hCREBH-F expression vector. Relative luciferase activities were shown as fold increases over the background levels shown by lysates prepared from control vector-transfected cells. Error bars are means ± S.D. of triplicates. N.S., not significant. ***, $P<0.001$. (C) Hepatocytes of Wild-type mice and CREBH-deficient mice were taken by a perfusion apparatus. Hepatocytes were transiently transfected with luciferase reporter plasmids containing the CYP2B10 promoter with Nr1 region together with

control or hCAR expression vector. Relative luciferase activities were shown as fold increases over the background levels shown by lysates prepared from control vector-transfected cells. Error bars are means ± S.D. of five ways. N.S., not significant. **, P<0.01; ***, P<0.001. Data are representative of three (B, C) independent experiments.
(TIF)

Figure S8 RNAi vector for CREBH suppressed the expression of CREBH *in vitro*. 293T cells were transfected with 2 μg HA-tagged mCREBH-F expression vectors together with indicated volumes of RNAi vectors targeting for mCREBH. At 24 hr after transfection, whole-cell lysates were prepared, and the knockdown efficiency of RNAi vectors for mCREBH was analysed by western blot analysis using anti-HA antibody. Data are representative of two independent experiments.
(TIF)

Table S1 A list of the sulpyrine-inducible genes studied.
(TIFF)

Table S2 Primers list used in this study.
(TIFF)

Acknowledgments

We thank C. Hidaka for excellent secretarial assistance; Y. Magota and M. Enomoto for technical assistance; and members of Takeda's lab for discussions.

Author Contributions

Conceived and designed the experiments: NK MY KT. Performed the experiments: NK MY HS JSM SM TK. Analyzed the data: NK MY KT. Contributed reagents/materials/analysis tools: MS JO YU HK. Wrote the paper: NK MY KT.

References

1. Malhi H, Kaufman RJ (2011) Endoplasmic reticulum stress in liver disease. J Hepatol 54: 795–809.
2. Hetz C, Glimcher LH (2009) Fine-tuning of the unfolded protein response: Assembling the IRE1alpha interactome. Mol Cell 35: 551–561.
3. Pavitt GD, Ron D (2012) New Insights into Translational Regulation in the Endoplasmic Reticulum Unfolded Protein Response. Cold Spring Harb Perspect Biol.
4. Harding HP, Zhang Y, Ron D (1999) Protein translation and folding are coupled by an endoplasmic-reticulum-resident kinase. Nature 397: 271–274.
5. Mori K (2010) Divest yourself of a preconceived idea: transcription factor ATF6 is not a soluble protein! Mol Biol Cell 21: 1435–1438.
6. Murakami T, Saito A, Hino S, Kondo S, Kanemoto S, et al. (2009) Signalling mediated by the endoplasmic reticulum stress transducer OASIS is involved in bone formation. Nat Cell Biol 11: 1205–1211.
7. Saito A, Hino S, Murakami T, Kanemoto S, Kondo S, et al. (2009) Regulation of endoplasmic reticulum stress response by a BBF2H7-mediated Sec23a pathway is essential for chondrogenesis. Nat Cell Biol 11: 1197–1204.
8. Nagamori I, Yomogida K, Ikawa M, Okabe M, Yabuta N, et al. (2006) The testes-specific bZip type transcription factor Tisp40 plays a role in ER stress responses and chromatin packaging during spermiogenesis. Genes Cells 11: 1161–1171.
9. Omori Y, Imai J, Watanabe M, Komatsu T, Suzuki Y, et al. (2001) CREB-H: a novel mammalian transcription factor belonging to the CREB/ATF family and functioning via the box-B element with a liver-specific expression. Nucleic Acids Res 29: 2154–2162.
10. Lee JH, Giannikopoulos P, Duncan SA, Wang J, Johansen CT, et al. (2011) The transcription factor cyclic AMP-responsive element-binding protein H regulates triglyceride metabolism. Nat Med 17: 812–815.
11. Luebke-Wheeler J, Zhang K, Battle M, Si-Tayeb K, Garrison W, et al. (2008) Hepatocyte nuclear factor 4alpha is implicated in endoplasmic reticulum stress-induced acute phase response by regulating expression of cyclic adenosine monophosphate responsive element binding protein H. Hepatology 48: 1242–1250.
12. Zhang K, Shen X, Wu J, Sakaki K, Saunders T, et al. (2006) Endoplasmic reticulum stress activates cleavage of CREBH to induce a systemic inflammatory response. Cell 124: 587–599.
13. Vecchi C, Montosi G, Zhang K, Lamberti I, Duncan SA, et al. (2009) ER stress controls iron metabolism through induction of hepcidin. Science 325: 877–880.
14. Lee MW, Chanda D, Yang J, Oh H, Kim SS, et al. (2010) Regulation of hepatic gluconeogenesis by an ER-bound transcription factor, CREBH. Cell Metab 11: 331–339.
15. Liska DJ (1998) The detoxification enzyme systems. Altern Med Rev 3: 187–198.
16. Hur KY, So JS, Ruda V, Frank-Kamenetsky M, Fitzgerald K, et al. (2012) IRE1alpha activation protects mice against acetaminophen-induced hepatotoxicity. J Exp Med 209: 307–318.
17. Gunawan BK, Liu ZX, Han D, Hanawa N, Gaarde WA, et al. (2006) c-Jun N-terminal kinase plays a major role in murine acetaminophen hepatotoxicity. Gastroenterology 131: 165–178.
18. Henderson NC, Pollock KJ, Frew J, Mackinnon AC, Flavell RA, et al. (2007) Critical role of c-jun (NH2) terminal kinase in paracetamol- induced acute liver failure. Gut 56: 982–990.
19. Geisslinger G, Bocker R, Levy M (1996) High-performance liquid chromatographic analysis of dipyrone metabolites to study their formation in human liver microsomes. Pharm Res 13: 1272–1275.
20. Pierre SC, Schmidt R, Brenneis C, Michaelis M, Geisslinger G, et al. (2007) Inhibition of cyclooxygenases by dipyrone. Br J Pharmacol 151: 494–503.
21. Swaminathan J, Ramalingam M, Sethuraman V, Sundaraganesan N, Sebastian S (2009) Vibrational spectroscopic studies and DFT calculations of 4-aminoantipyrine. Spectrochim Acta A Mol Biomol Spectrosc 73: 593–600.
22. Kraul H, Truckenbrodt J, Huster A, Topfer R, Hoffmann A (1991) Comparison of in vitro and in vivo biotransformation in patients with liver disease of differing severity. Eur J Clin Pharmacol 41: 475–480.
23. Henschel L, Hoffmann A (1991) [Assessment of biotransformation capacity following oral administration of various model substances as cocktail]. Z Gastroenterol 29: 645–649.
24. Lautenschlager MT, Viktor S, Muller UA, Hoffmann A (1996) [Comparison of serum concentrations of caffeine, 4-methylaminoantipyrine, sulfamethazine and debrisoquin following oral administration of these substances as a cocktail in type II diabetics before and after insulin therapy]. Pharmazie 51: 750–753.
25. Honkakoski P, Zelko I, Sueyoshi T, Negishi M (1998) The nuclear orphan receptor CAR-retinoid X receptor heterodimer activates the phenobarbital-responsive enhancer module of the CYP2B gene. Mol Cell Biol 18: 5652–5658.
26. Sueyoshi T, Kawamoto T, Zelko I, Honkakoski P, Negishi M (1999) The repressed nuclear receptor CAR responds to phenobarbital in activating the human CYP2B6 gene. J Biol Chem 274: 6043–6046.
27. Zelko I, Negishi M (2000) Phenobarbital-elicited activation of nuclear receptor CAR in induction of cytochrome P450 genes. Biochem Biophys Res Commun 277: 1–6.
28. Wei P, Zhang J, Egan-Hafley M, Liang S, Moore DD (2000) The nuclear receptor CAR mediates specific xenobiotic induction of drug metabolism. Nature 407: 920–923.
29. Moore LB, Parks DJ, Jones SA, Bledsoe RK, Consler TG, et al. (2000) Orphan nuclear receptors constitutive androstane receptor and pregnane X receptor share xenobiotic and steroid ligands. J Biol Chem 275: 15122–15127.
30. Swales K, Kakizaki S, Yamamoto Y, Inoue K, Kobayashi K, et al. (2005) Novel CAR-mediated mechanism for synergistic activation of two distinct elements within the human cytochrome P450 2B6 gene in HepG2 cells. J Biol Chem 280: 3458–3466.
31. Chin KT, Zhou HJ, Wong CM, Lee JM, Chan CP, et al. (2005) The liver-enriched transcription factor CREB-H is a growth suppressor protein under-expressed in hepatocellular carcinoma. Nucleic Acids Res 33: 1859–1873.
32. Tekkok IH (2011) Metamizole is not as safe as we think or assume. Turk Neurosurg 21: 116–117.
33. Wessel JC, Matyja M, Neugebauer M, Kiefer H, Daldrup T, et al. (2006) Characterization of oxalic acid derivatives as new metabolites of metamizol (dipyrone) in incubated hen's egg and human. Eur J Pharm Sci 28: 15–25.
34. Gladtke E (1983) Use of antipyretic analgesics in the pediatric patient. Am J Med 75: 121–126.
35. Fendrich Z (2000) [Metamizol–a new effective analgesic with a long history. Overview of its pharmacology and clinical use]. Cas Lek Cesk 139: 440–444.
36. Janke C, Schmeck J, Passani D, Dodidou P, Stuck B, et al. (2003) [Anaphylactic cardiocirculatory failure after intraoperative application of dipyrone]. Anaesthesist 52: 321–325.
37. Jaszczuk E, Graczyk M, Oszukowski P, Brzezinski P (1999) [Anaphylactic shock leading to death in a young woman after oral administration of metamizole (Pyralginum-Polfa)–case report]. Przegl Lek 56: 175–176.
38. Volz M, Kellner HM (1980) Kinetics and metabolism of pyrazolones (propyphenazone, aminopyrine and dipyrone). Br J Clin Pharmacol 10 Suppl 2: 299S–308S.
39. Reznik ND, Rumiatseva EP, Borisova AP (1972) [Anaphylactic shock due to the use of amidopyrine]. Klin Med (Mosk) 50: 133.
40. Raucy JL, Lasker JM, Lieber CS, Black M (1989) Acetaminophen activation by human liver cytochromes P450IIE1 and P450IA2. Arch Biochem Biophys 271: 270–283.

41. Zaher H, Buters JT, Ward JM, Bruno MK, Lucas AM, et al. (1998) Protection against acetaminophen toxicity in CYP1A2 and CYP2E1 double-null mice. Toxicol Appl Pharmacol 152: 193–199.
42. James LP, Mayeux PR, Hinson JA (2003) Acetaminophen-induced hepatotoxicity. Drug Metab Dispos 31: 1499–1506.
43. Cohen SD, Khairallah EA (1997) Selective protein arylation and acetaminophen-induced hepatotoxicity. Drug Metab Rev 29: 59–77.
44. Okamura M, Takano Y, Hiramatsu N, Hayakawa K, Yao J, et al. (2008) Suppression of cytokine responses by indomethacin in podocytes: a mechanism through induction of unfolded protein response. Am J Physiol Renal Physiol 295: F1495–1503.
45. Tsutsumi S, Gotoh T, Tomisato W, Mima S, Hoshino T, et al. (2004) Endoplasmic reticulum stress response is involved in nonsteroidal anti-inflammatory drug-induced apoptosis. Cell Death Differ 11: 1009–1016.
46. Tsutsumi S, Namba T, Tanaka KI, Arai Y, Ishihara T, et al. (2006) Celecoxib upregulates endoplasmic reticulum chaperones that inhibit celecoxib-induced apoptosis in human gastric cells. Oncogene 25: 1018–1029.
47. Yang H, Park SH, Choi HJ, Moon Y (2010) The integrated stress response-associated signals modulates intestinal tumor cell growth by NSAID-activated gene 1 (NAG-1/MIC-1/PTGF-beta). Carcinogenesis 31: 703–711.
48. Singh G (1998) Recent considerations in nonsteroidal anti-inflammatory drug gastropathy. Am J Med 105: 31S–38S.
49. Din FV, Theodoratou E, Farrington SM, Tenesa A, Barnetson RA, et al. (2010) Effect of aspirin and NSAIDs on risk and survival from colorectal cancer. Gut 59: 1670–1679.
50. Johannesdottir SA, Chang ET, Mehnert F, Schmidt M, Olesen AB, et al. (2012) Nonsteroidal anti-inflammatory drugs and the risk of skin cancer: A population-based case-control study. Cancer.
51. Namba T, Homan T, Nishimura T, Mima S, Hoshino T, et al. (2009) Up-regulation of S100P expression by non-steroidal anti-inflammatory drugs and its role in anti-tumorigenic effects. J Biol Chem 284: 4158–4167.
52. Mizushima T (2008) [Strategy for development of NSAIDs with lower risk for side effects]. Yakugaku Zasshi 128: 255–261.
53. Tanaka K, Tomisato W, Hoshino T, Ishihara T, Namba T, et al. (2005) Involvement of intracellular Ca2+ levels in nonsteroidal anti-inflammatory drug-induced apoptosis. J Biol Chem 280: 31059–31067.
54. Eggan K, Akutsu H, Loring J, Jackson-Grusby L, Klemm M, et al. (2001) Hybrid vigor, fetal overgrowth, and viability of mice derived by nuclear cloning and tetraploid embryo complementation. Proc Natl Acad Sci U S A 98: 6209–6214.
55. Katz EZ, Granit L, Drayer DE, Levy M (1984) Simultaneous determination of dipyrone metabolites in plasma by high-performance liquid chromatography. J Chromatogr 305: 477–484.
56. Ponomarev ED, Veremeyko T, Barteneva N, Krichevsky AM, Weiner HL (2011) MicroRNA-124 promotes microglia quiescence and suppresses EAE by deactivating macrophages via the C/EBP-alpha-PU.1 pathway. Nat Med 17: 64–70.
57. Adachi O, Kawai T, Takeda K, Matsumoto M, Tsutsui H, et al. (1998) Targeted disruption of the MyD88 gene results in loss of IL-1- and IL-18-mediated function. Immunity 9: 143–150.
58. Tamaki N, Hatano E, Taura K, Tada M, Kodama Y, et al. (2008) CHOP deficiency attenuates cholestasis-induced liver fibrosis by reduction of hepatocyte injury. Am J Physiol Gastrointest Liver Physiol 294: G498–505.
59. Yamamoto M, Sato S, Hemmi H, Hoshino K, Kaisho T, et al. (2003) Role of adaptor TRIF in the MyD88-independent toll-like receptor signaling pathway. Science 301: 640–643.

THE JOURNAL OF IMMUNOLOGY

Ecto-Nucleoside Triphosphate Diphosphohydrolase 7 Controls Th17 Cell Responses through Regulation of Luminal ATP in the Small Intestine

Takashi Kusu, Hisako Kayama, Makoto Kinoshita, Seong Gyu Jeon, Yoshiyasu Ueda, Yoshiyuki Goto, Ryu Okumura, Hiroyuki Saiga, Takashi Kurakawa, Kayo Ikeda, Yuichi Maeda, Jun-ichi Nishimura, Yasunobu Arima, Koji Atarashi, Kenya Honda, Masaaki Murakami, Jun Kunisawa, Hiroshi Kiyono, Meinoshin Okumura, Masahiro Yamamoto and Kiyoshi Takeda

J Immunol 2013; 190:774-783; Prepublished online 14 December 2012;
doi: 10.4049/jimmunol.1103067
http://www.jimmunol.org/content/190/2/774

The Journal of Immunology is published twice each month by The American Association of Immunologists, Inc., 9650 Rockville Pike, Bethesda, MD 20814-3994.

Print ISSN: 0022-1767 Online ISSN: 1550-6606.

Ecto-Nucleoside Triphosphate Diphosphohydrolase 7 Controls Th17 Cell Responses through Regulation of Luminal ATP in the Small Intestine

Takashi Kusu,[*,†] Hisako Kayama,[*,‡,§] Makoto Kinoshita,[*,§] Seong Gyu Jeon,[*,‡] Yoshiyasu Ueda,[*] Yoshiyuki Goto,[¶] Ryu Okumura,[*,‡] Hiroyuki Saiga,[*] Takashi Kurakawa,[*] Kayo Ikeda,[*,‡] Yuichi Maeda,[*,‡] Jun-ichi Nishimura,[*] Yasunobu Arima,[‖] Koji Atarashi,[*] Kenya Honda,[*] Masaaki Murakami,[§,‖] Jun Kunisawa,[¶,#] Hiroshi Kiyono,[§,¶] Meinoshin Okumura,[†] Masahiro Yamamoto,[*,‡,§] and Kiyoshi Takeda[*,‡,§]

Extracellular ATP is released from live cells in controlled conditions, as well as dying cells in inflammatory conditions, and, thereby, regulates T cell responses, including Th17 cell induction. The level of extracellular ATP is closely regulated by ATP hydrolyzing enzymes, such as ecto-nucleoside triphosphate diphosphohydrolases (ENTPDases). ENTPDase1/CD39, which is expressed in immune cells, was shown to regulate immune responses by downregulating the ATP level. In this study, we analyzed the immunomodulatory function of ENTPDase7, which is preferentially expressed in epithelial cells in the small intestine. The targeted deletion of *Entpd7* encoding ENTPDase7 in mice resulted in increased ATP levels in the small intestinal lumen. The number of Th17 cells was selectively increased in the small intestinal lamina propria in *Entpd7*$^{-/-}$ mice. Th17 cells were decreased by oral administration of antibiotics or the ATP antagonist in *Entpd7*$^{-/-}$ mice, indicating that commensal microbiota-dependent ATP release mediates the enhanced Th17 cell development in the small intestinal lamina propria of *Entpd7*$^{-/-}$ mice. In accordance with the increased number of small intestinal Th17 cells, *Entpd7*$^{-/-}$ mice were resistant to oral infection with *Citrobacter rodentium*. *Entpd7*$^{-/-}$ mice suffered from severe experimental autoimmune encephalomyelitis, which was associated with increased numbers of CD4^{+} T cells producing both IL-17 and IFN-γ. Taken together, these findings demonstrate that ENTPDase7 controls the luminal ATP level and, thereby, regulates Th17 cell development in the small intestine. *The Journal of Immunology*, **2013, 190: 774–783.**

Extracellular ATP was shown to modulate cellular functions via purinergic receptors in the nervous, vascular, and immune system (1–3). In the immune system, the purinergic receptors, such as P2X7 and P2Y2, recognize ATP that is released from damaged and dying cells. P2X7-dependent sensing of ATP leads to activation of the NALP3 inflammasome that induces inflammation via production of IL-1β/IL-18 (4, 5). P2Y2 was shown to mediate recruitment of neutrophils and macrophages into inflammatory sites and clearance of apoptotic cells by phagocytes (6–8). Thus, the innate immune system recognizes extracellular ATP as danger signals to regulate inflammatory responses. In addition to ATP that is released from damaged cells, ATP is released from intact cells under normal conditions and modulates various immune-cellular functions, such as maturation of dendritic cells (DCs) and activation of B and T cells (3, 9). Recently, several reports indicated that ATP modulates mucosal immune responses by influencing the function of intestinal epithelial cells (ECs) and T cells (10–13). Extracellular ATP was also shown to directly modulate T cell responses through P2X receptors, leading to the induction of intestinal inflammation (14, 15).

Therefore, the level of extracellular ATP is closely regulated to prevent uncontrolled ATP-mediated cellular responses by surface-expressing enzymes that hydrolyze ATP, such as members of the ecto-nucleoside triphosphate diphosphohydrolase (ENTPDase) family, consisting of eight members (ENTPDase1–8) (16–18). Among them, ENTPDase1 (also known as CD39), which is highly

*Laboratory of Immune Regulation, Department of Microbiology and Immunology, Graduate School of Medicine, Osaka University, Suita, Osaka 565-0871, Japan; †Department of General Thoracic Surgery, Graduate School of Medicine, Osaka University, Suita, Osaka 565-0871, Japan; ‡Laboratory of Mucosal Immunology, World Premier International Immunology Frontier Research Center, Osaka University, Suita, Osaka 565-0871, Japan; §Core Research for Evolutional Science and Technology, Japan Science and Technology Agency, Saitama 332-0012, Japan; ¶Division of Mucosal Immunology, Department of Microbiology and Immunology, Institute of Medical Science, University of Tokyo, Tokyo 108-8639, Japan; ‖Laboratory of Developmental Immunology, Graduate School of Frontier Biosciences, Graduate School of Medicine and World Premier International Immunology Frontier Research Center, Osaka University, Osaka 565-0871, Japan; and #Laboratory of Vaccine Materials, National Institute of Biomedical Innovation, Osaka 567-0085, Japan

Received for publication October 25, 2011. Accepted for publication November 8, 2012.

This work was supported by a Grant-in-Aid from the Ministry of Education, Culture, Sports, Science and Technology; the Ministry of Health, Labour and Welfare; and the Osaka Foundation for the Promotion of Clinical Immunology.

Address correspondence and reprint requests to Prof. Kiyoshi Takeda, Laboratory of Immune Regulation, Department of Microbiology and Immunology, Graduate School of Medicine, Osaka University, Suita, Osaka 565-0871, Japan. E-mail address: ktakeda@ongene.med.osaka-u.ac.jp

The online version of this article contains supplemental material.

Abbreviations used in this article: DC, dendritic cell; EAE, experimental autoimmune encephalomyelitis; EC, epithelial cell; ENTPDase, ecto-nucleoside triphosphate diphosphohydrolase; MLN, mesenteric lymph node; MOG, myelin oligodendrocyte glycoprotein; oATP, oxidized ATP; SFB, segmented filamentous bacteria.

www.jimmunol.org/cgi/doi/10.4049/jimmunol.1103067

expressed in immune cells, such as T cells, B cells, NK cells, DCs, and monocytes/macrophages (19, 20), was shown to possess anti-inflammatory activities through ATP hydrolysis. Indeed, severe inflammation was induced in mice lacking ENTPDase1/CD39 in several inflammatory models, including inflammatory bowel disease (21–24). Combinational activity of ENTPDases such as CD39 with CD73 ecto-5′-nucleotidase, which hydrolyzes AMP to adenosine, was also demonstrated in regulatory T cells and intestinal ECs (11, 20, 25). Thus, the immune-modulatory functions of ENTPDase1/CD39 have been well characterized. However, it remains unclear whether other ENTPDase family members are involved in the regulation of immune responses.

In this study, we analyzed the role of ENTPDase7, which was selectively expressed in ECs in the small intestine. Deletion of ENTPDase7 in mice resulted in increased ATP concentrations in the small intestinal lumen and increased numbers of IL-17–producing Th17 cells in the small intestinal lamina propria. Blockade of ATP action decreased the number of Th17 cells in the small intestine of ENTPDase7-deficient mice. In accordance with the increased Th17 cell number, ENTPDase7-deficient mice showed high resistance to the intestinal pathogen *Citrobacter rodentium*. These findings demonstrate that intestinal ECs participate in the regulation of Th17 cell responses by controlling intestinal ATP levels.

Materials and Methods

Real-time RT-PCR

RNA samples were prepared from various organs, epithelial layer, and lamina propria of C57BL/6J mice (CLEA Japan) using TRIzol reagent (Invitrogen), from single-cell suspensions using an RNeasy Mini Kit (QIAGEN), or from laser-microdissected tissue sections using an RNeasy Micro Kit (QIAGEN). Total RNA was reverse transcribed using Moloney murine leukemia virus reverse transcriptase (Promega) and random primers (Toyobo) after treatment with RQ1 DNase I (Promega). cDNA was analyzed by real-time RT-PCR using GoTaq qPCR Master Mix (Promega) in an ABI 7300 real-time PCR system (Applied Biosystems). Values were then normalized to the expression of *Gapdh*, and the fold difference in expression relative to that of *Gapdh* is shown. The following primer sets were used: *Entpd1*, 5′-TGGTGCAGCAGTTAGAGGAATG-3′ and 5′-CGCACCGATTTCATCTGTTTT-3′; *Entpd7*, 5′-CCCCTTTACATCCTCTGCAC-3′ and 5′-GTCAAACTCCAACGGCAAAT-3′; *Muc2*, 5′-ACATCACCTGTCCCGACTTC-3′ and 5′-GAGCAAGGGACTCTGGTCTG-3′; *Krt7*, 5′-ACGGCTGCTGAGAATGAGTT-3′ and 5′-CGTGAAGGGTCTTGAGGAAG-3′; and *Gapdh*, 5′-CCTCGTCCCGTAGACAAAATG-3′ and 5′-TCTCCACTTTGCCACTGCAA-3′.

Isolation of epithelium and lamina propria

Intestines were opened longitudinally, washed to remove fecal content, and incubated in PBS containing 30 mM EDTA for 5 min. Epithelial layer was peeled off from intestines and used as epithelium. For isolation of lamina propria, after removing the epithelial layer, fat tissue was also removed from intestines.

Laser microdissection

The frozen sections (10 μm) of the small intestine were fixed with acetic acid/ethyl alcohol (1:19) for 3 min, followed by H&E staining. Tissues containing >100 goblet cells, absorptive enterocytes, and lamina propria cells were collected by a laser microdissection device (DM6000B; Leica, Tokyo, Japan).

Generation of Entpd7-deficient mice

The targeting vector was constructed by replacement of a 1.0-kb fragment encoding the fourth and fifth exons of *Entpd7* with a neomycin resistance gene cassette, and a gene encoding HSV thymidine kinase driven by a phosphoglycerate kinase promoter was inserted into the genomic fragment for negative selection. After the targeting vector was transfected into V6.5 embryonic stem cells, G418 and ganciclovir double-resistant colonies were selected and screened by PCR and Southern blot analysis. Homologous recombinants were microinjected into blastocysts of C57BL/6 female mice, and heterozygous F1 progeny mice were intercrossed to obtain *Entpd7*-deficient mice. *Entpd7*-deficient mice and their wild-type littermates from these intercrosses were confirmed by Southern blot analysis and Northern blot analysis and were used for experiments. *Entpd7*-deficient mice were backcrossed onto C57BL/6 mice for at least four generations, and *Entpd7*-deficient mice and their wild-type littermates from intercrosses of heterozygous mice were used for experiments. All animal experiments were conducted in accordance with the guidelines of the Animal Care and Use Committee of Osaka University.

Isolation of lymphocytes

To prepare single-cell suspensions from spleens, mesenteric lymph nodes (MLNs), and Peyer's patches, the collected organs were ground between glass slides, and the cells were passed through 40-μm nylon meshes and suspended in PBS. Splenocytes were treated with RBC lysis buffer (0.15 M NH_4Cl, 1 mM $KHCO_3$, 0.1 mM EDTA) for 5 min before suspension. Naive $CD4^+$ T cells were purified using a FACSAria system as $CD4^+CD25^-CD44^{low}CD62L^{high}$ cells. For isolation of intraepithelial lymphocytes, intestines were opened longitudinally, washed to remove fecal content, and shaken in HBSS containing 5 mM EDTA for 20 min at 37°C. After filtration through nylon mesh, the EC fraction was washed with RPMI 1640 containing 4% FBS, resuspended in 5 ml 40% Percoll (GE Healthcare), and overlaid on 2.5 ml 80% Percoll in a 15-ml Falcon tube. Percoll-gradient separation was performed by centrifugation at 780 × *g* for 20 min at 25°C. The intraepithelial lymphocytes were collected at the interface of the Percoll gradient and washed with RPMI 1640 containing 10% FBS. For isolation of lamina propria lymphocytes, intestines were opened, washed to remove fecal content, shaken in HBSS containing 5 mM EDTA for 20 min at 37°C to remove ECs and fat tissue, cut into small pieces, and incubated with RPMI 1640 containing 4% FBS, 1 mg/ml collagenase D (Roche), 0.5 mg/ml dispase (Invitrogen), and 40 μg/ml DNase I (Roche) for 1 h at 37°C in a shaking water bath. The digested tissues were washed with HBSS containing 5 mM EDTA and subjected to Percoll density-gradient centrifugation as for isolation of intraepithelial lymphocytes. The lamina propria lymphocytes were collected at the interface of the Percoll gradient and washed with RPMI 1640 containing 10% FBS.

Intracellular cytokine staining

Intracellular expression of IL-17, IFN-γ, and IL-10 in $CD4^+$ T cells was analyzed using a Cytofix/Cytoperm Kit Plus (with GolgiStop; BD Biosciences), according to the manufacturer's instructions. In brief, lymphocytes obtained from the intestinal lamina propria, spleens, MLNs, or Peyer's patches were incubated with 50 ng/ml PMA (Sigma), 5 μM calcium ionophore A23187 (Sigma), and GolgiStop at 37°C for 4 h. Surface staining was performed with anti-CD4-PerCP/Cy5.5 (BioLegend) for 20 min at 4°C, the cells were permeabilized with Cytofix/Cytoperm solution for 20 min at 4°C, and intracellular cytokine staining was performed with anti–IL-17A–Alexa Fluor 647 (BD Biosciences), anti–IL-10–PE (BD Biosciences), and anti–IFN-γ–FITC (BioLegend) for 20 min. For intracellular staining of Foxp3, cells were stained using the Foxp3 Staining Buffer set (eBiosciences).

Flow cytometry

The following Abs were used for flow cytometry: anti–CD4-PerCP/Cy5.5, anti–CD8α–Pacific Blue, anti–CD3-FITC, anti–TCRγδ-PE, anti–TCRβ-FITC, anti–CD8β–Alexa Fluor 647, and anti–CD4-PE/Cy7 (all from BioLegend); anti–B220-PE, anti–CD3-PE/Cy7, and anti–CD8α-PE (all from BD Biosciences); and anti–TCRγδ-FITC (eBioscience). Anti–Foxp3–Alexa Fluor 647 (eBioscience) was also used, according to the manufacturer's instructions. Data were acquired using a FACSCanto II (BD Biosciences) and analyzed using FlowJo software (Tree Star).

Establishment of small intestinal EC lines

H-2Kb-tsA58–transgenic mice (26) were backcrossed to C57BL/6 mice for six generations. To establish the small intestinal EC lines from wild-type and $Entpd7^{-/-}$ mice, the mice were crossed with H-2Kb-tsA58–transgenic mice. Small intestinal ECs were isolated, as previously described (27), before incubation at 33°C. To confirm that they were intestinal ECs, a single-cell suspension was prepared and cytospun onto the glass slides. After fixation, the cells were incubated with polyclonal anti-cytokeratin Ab (1:500; Dako) and then treated with a ChemMate EnVision kit (Dako). DAB (Dako) was used as a chromogen. Images were taken using a BZ-9000 fluorescence microscope (Keyence).

Measurement of ATP

Feces from individual mice were collected, weighed, and gently suspended in PBS containing 0.01% NaN_3. After centrifugation, the supernatants were collected, and the levels of ATP were determined with a luciferin-

luciferase assay using the ATP assay kit (Toyo Ink), according to the manufacturer's instructions. To analyze ATP levels in the small intestinal tissues, the small intestine was isolated and cut into quarters longitudinally. Each piece was weighed and lysed to measure ATP with a luciferin-luciferase assay. To analyze ATP levels in the EC lines, single-cell suspensions of the indicated cell lines were prepared. The cells were counted and lysed to measure ATP with a luciferin-luciferase assay. For determination of luminal ATP levels, the mice were fasted overnight and anesthetized by i.p. injection with 350 μl 0.5% pentobarbital sodium (Dainippon Sumitomo Pharma). The peritoneal cavity was opened, and the small intestine was ligated with nylon threads at 1.5 and 4.5 cm distal from the Treitz ligament (for the proximal region of the small intestine) or at 3 and 6 cm proximal from the ileum end (for the distal region of the small intestine) to make a closed intestinal loop. A total of 300 ml PBS or 1.5 mM ATP solution was applied luminally with a 29-G needle. The luminal fluid was recovered 15 min later using a 29-G needle and suspended in PBS. After centrifugation, the supernatants were collected, and the levels of ATP were determined with a luciferin-luciferase assay.

Measurement of NTP hydrolyzing activity

NTP (ATP, GTP, UTP, and CTP) hydrolyzing activity was measured in crude membranes from wild-type and *Entpd7*$^{-/-}$ small intestinal ECs, as previously described (28). Briefly, ECs were homogenized; after removing nuclei, the crude membrane fraction was separated from the cytosol by centrifugation at 100,000 × *g* for 30 min. To assay NTP hydrolyzing activity, the membrane fraction containing 10 μg total protein was suspended in reaction buffer (20 mM HEPES [pH 7.4], 120 mM NaCl, 5 mM KCl, 0.2 mM EDTA, 1 mM NaN_3, and 0.5 mM Na_3VO_4, with or without 5 mM $CaCl_2$). After incubation for 5 min at 37°C, 5 μl the reaction buffer containing 10 mM NTP was added and incubated for 30 min. NTP hydrolyzing activity was determined by measuring the inorganic phosphate, as described previously (28).

In vitro naive T cell differentiation

Naive T cells were grown for 4 d at 5 × 10^5 cells/ml with plate-bound anti-CD3 (2 mg/ml) in DMEM supplemented with 10% FBS, penicillin, and streptomycin under Th17-polarizing conditions (2 ng/ml TGF-β, 20 ng/ml IL-6, 5 μg/ml anti–IFN-γ, 5 μg/ml anti–IL-4) or Th0 conditions (5 μg/ml anti–IFN-γ, 5 μg/ml anti–IL-4). Then, cells were incubated with 50 ng/ml PMA (Sigma), 5 μM calcium ionophore A23187 (Sigma), and GolgiStop at 37°C for 4 h for flow cytometry analysis.

Treatment with antibiotics

Mice were given a combination of antibiotics containing 500 μg/ml vancomycin (Wako), 1 mg/ml metronidazole, 1 mg/ml ampicillin, and 1 mg/ml neomycin sulfate (all from Nacalai Tesque) in drinking water from birth for 8 wk prior to flow cytometric analysis of the small intestinal lamina propria $CD4^+$ lymphocytes.

Isolation of bacterial DNA

The isolation of bacterial DNA was performed as previously described (29), with some modifications. Briefly, small intestines isolated from littermate mice at 10 wk of age were opened longitudinally, and intestinal contents were collected. Intestinal tissues were washed three times with PBS for 10 s to remove the mucus layer. To collect epithelium-associated bacteria, tissues were further treated by vigorous hand shaking three times for 20 s in PBS containing 0.5% Tween 20 (30). After centrifuging, pellets were suspended in 500 μl TE buffer (10 mM Tris-HCl, 1 mM EDTA [pH 8]). Glass beads and extraction buffer containing TE-saturated phenol and $NaDodSO_4$ solutions were added to the suspension. The mixture was shaken vigorously on a FastPrep FP100 A (BIO 101); this step was repeated after incubation for 10 min at 65°C. After centrifugation, bacterial DNA was precipitated with isopropanol, washed with 70% ethanol, and suspended in 50 μl TE buffer.

Quantitative real-time PCR amplification of 16S rRNA gene sequences

For quantitative analysis of specific bacterial groups in the luminal contents and epithelial layer of the small intestine, quantitative real-time PCR was performed using a LightCycler 480 II (Roche). Bacterial 16S rRNA genes extracted from luminal contents and epithelial surfaces were amplified by bacterial group–specific primers: all bacteria, 5′-ACTCCTACGGGAGGCAGCAGT-3′ and 5′-ATTACCGCGGCTGCTGGC-3′; Lactobacillaceae, 5′-AGCAGTAGGGAATCTTCCA-3′ and 5′-CACCGCTACACATGGAG-3′; segmented filamentous bacteria (SFB), 5′-GACGCTGAGGCATGAGAGCAT-3′ and 5′-GACGGCACGGATTGTTATTCA-3′; *Bacteroides*, 5′-GGTTCTGAGAGGAAGGTCCC-3′ and 5′-GCTGCCTCCCGTAGGAGT-3′; and Clostridiales, 5′-ACTCCTACGGGAGGCAGC-3′ and 5′-GCTTCTTAGTCAGGTACCGTCAT-3′ (31, 32). All reactions were performed in 20 μl using SYBR Green I Master Mix (Roche). Absolute numbers of bacterial 16S rRNA gene copies were determined from standard curves constructed by quantitative PCR of reference plasmids, including 16S rRNA genes isolated from *Lactobacillus johnsonii*, a type strain of *Lactobacillus* obtained from Japan Collection of Microorganisms (JCM No. 2012), murine intestinal *Bacteroides*, *Clostridium*, and SFB.

Treatment with oxidized ATP

Mice were given 100 μl 6 mM oxidized ATP (oATP; ATP periodate oxidized sodium salt; Sigma) i.v. daily for 2 wk prior to flow cytometric analysis of the small intestinal lamina propria $CD4^+$ lymphocytes.

C. rodentium *infection*

C. rodentium (NBRC 105723T) was cultured in Luria–Bertani broth at 37°C for 16 h. Wild-type and *Entpd7*-deficient mice were infected orally with 2 × 10^9 *C. rodentium* in a total volume of 200 μl/mouse. Survival of infected mice was monitored. At 14 d after the infection, spleens were isolated, weighed, and homogenized. Serial dilutions of the homogenates with saline were spread onto MacConkey agar (Merck). After incubation at 37°C for 16 h, the colonies of the appropriate dilutions were counted, and the CFU of bacteria per gram of tissues was calculated. *C. rodentium* colonies were identified as pink colonies.

Experimental autoimmune encephalomyelitis induction in mice

For the induction of experimental autoimmune encephalomyelitis (EAE), mice were immunized s.c. with 100 μg myelin oligodendrocyte glycoprotein $(MOG)_{35-55}$ (Biologica) in 100 μl CFA (Difco) divided among four sites, two on each hind flank. Then, the mice received 250 ng *Bordetella pertussis* toxin (List Biological Laboratories) i.p. on days 0 and 2. The CNS, especially the whole brain and spinal cord, was harvested 17 d after challenge, cut into pieces, and incubated in DMEM containing 2.5 mg/ml collagenase D (Roche) and 1 mg/ml DNase I (Roche) for 20 min at 37°C in a shaking water bath. The digested tissues were resuspended in 5 ml 37% Percoll (GE Healthcare) and then overlaid on 2.5 ml 70% Percoll in a 15-ml tube. Percoll-gradient separation was performed by centrifugation at 500 × *g* for 20 min at room temperature. Lymphocytes were collected at the Percoll gradient interface and washed with RPMI 1640 containing 10% FBS. Mice were assigned scores of 1 to 5 as follows: 0, no clinical signs of EAE; 1, paralyzed tail; 2, loss of coordinated movement; 3, both hind limbs paralyzed; 4, forelimbs paralyzed; and 5, moribund.

Statistical analysis

Differences between control and experimental groups were evaluated by the Student *t* test.

Results

Selective expression of Entpd7 in small intestinal epithelia

ENTPDase1/CD39 encoded by *Entpd1* was shown to modulate inflammatory responses in addition to thrombopoiesis (24, 33, 34). Because the ENTPDase family consists of eight members, we analyzed tissue expression of *Entpd* gene family members. *Entpd1* was preferentially expressed in lymphoid organs, such as the spleen and lymph nodes (Fig. 1A). Of the other *Entpd* genes, we focused on those that showed selective tissue-expression patterns. *Entpd7* was highly expressed in the small intestine (Fig. 1B). The highest *Entpd7* expression was observed in the proximal region of the small intestine, and its expression gradually decreased as the small intestines descended (Fig. 1C). We then analyzed expression of *Entpd7* in the epithelial layers and lamina propria of the small intestine (Fig. 1D). *Entpd7* was predominantly expressed in the ECs of the small intestine. We further analyzed which types of intestinal ECs (i.e., goblet cells or absorptive enterocytes) highly expressed *Entpd7*. Goblet cell–enriched, absorptive enterocyte-enriched, and lamina propria cell–enriched regions were isolated by laser microdissection, and expression of *Entpd7* was analyzed (Fig. 1E). *Entpd7* was highly expressed in absorptive enterocytes, as well as goblet cells characterized by high expression of *Muc2*.

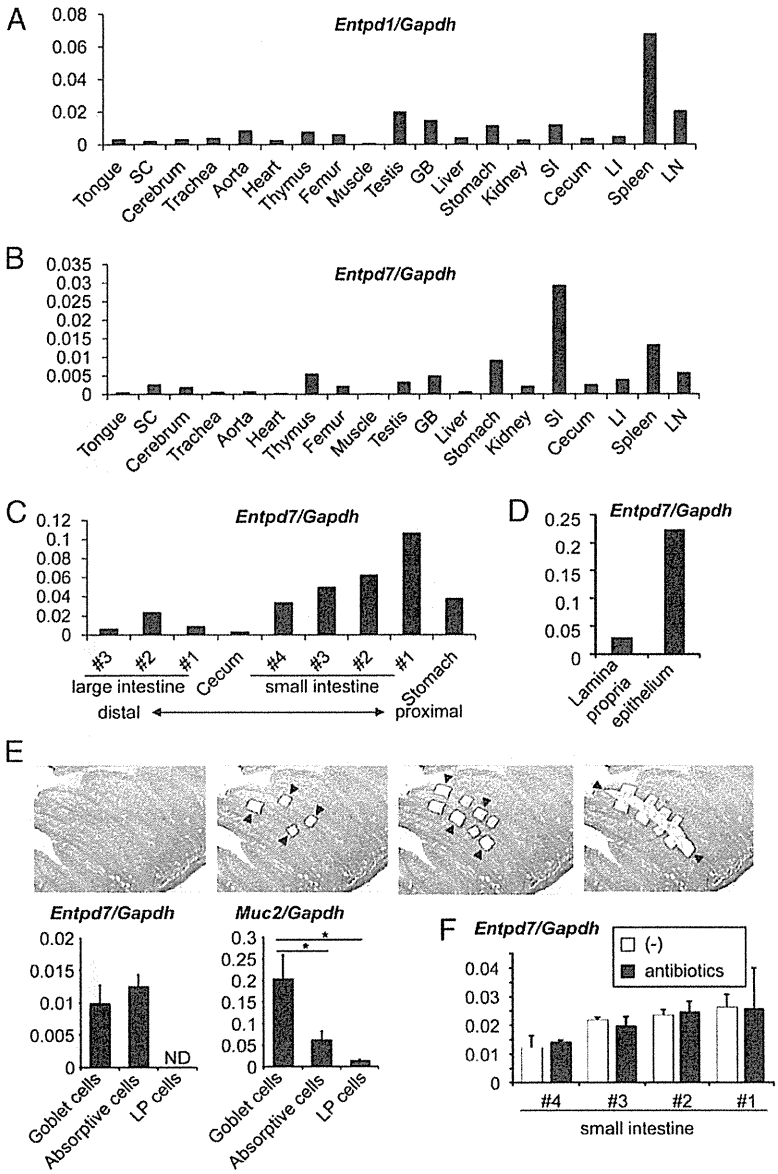

FIGURE 1. High *Entpd7* expression in epithelium of the small intestine. Real-time quantitative RT-PCR analysis of mRNA expression of *Entpd1* (**A**) and *Entpd7* (**B**) in various organs. RNA samples were prepared from various organs of C57BL/6J mice and analyzed by real-time RT-PCR. The values were normalized to that of *Gapdh*. (**C**) Real-time quantitative RT-PCR analysis of *Entpd7* expression in the alimentary tract. The small intestine was cut transversely into four equal pieces, and the colon was cut into three equal pieces. The smaller number denotes the more proximal site of the intestine. Data are representative of three independent experiments. (**D**) Real-time quantitative RT-PCR analysis of *Entpd7* expression in the epithelium and lamia propria of the small intestine. The values were normalized to that of *Gapdh*. Data are representative of three independent experiments. Real-time quantitative RT-PCR analysis of *Entpd7* expression in goblet cells, absorptive ECs, and lamina propria (LP) cells (**E**) and the epithelium of the small intestine (**F**) in mice treated with oral antibiotics. Goblet cell–, absorptive cell–, and lamina propria cell–enriched regions were isolated by laser microdissection. Each region is indicated by arrowheads. H&E staining. Original magnification ×50. The expression of *Muc2*, encoding mucin-2, was also analyzed. The values were normalized to that of *Gapdh*. Data are representative of two independent experiments and represent mean + SD of three mice. $*p < 0.05$. GB, Gall bladder; LI, large intestine; LN, mesenteric lymph node; SC, spinal cord; SI, small intestine.

Thus, *Entpd7* is highly expressed in all types of ECs of the small intestine. Expression of *Entpd7* in the small intestine was not altered in mice treated with oral antibiotics, indicating that *Enptd7* expression is not influenced by microbiota (Fig. 1F).

To assess the physiological function of ENTPDase7 encoded by *Entpd7*, we generated *Entpd7*$^{-/-}$ mice by gene targeting (Supplemental Fig. 1A, 1B). *Entpd7*$^{-/-}$ mice were born at the normal Mendelian ratios and grew healthily until 16 wk of age (Supplemental Fig. 1C). Normal lymphocyte development was observed in *Entpd7*$^{-/-}$ mice (Supplemental Fig. 1D). The composition of lymphocytes in the small and large intestine was not altered in *Entpd7*$^{-/-}$ mice (Supplemental Fig. 2).

Elevated ATP level in the small intestinal lumen of Entpd7$^{-/-}$ *mice*

Because ENTPDase is an enzyme that hydrolyzes nucleoside triphosphates, and *Entpd7* was selectively expressed in the small intestinal epithelia, we analyzed concentrations of ATP in the intestine. First, the small intestines were cut into four regions, and their lysates were analyzed for ATP concentration (Fig. 2A). The ATP level was not dramatically altered in any region of the small intestinal tissues between wild-type and *Entpd7*$^{-/-}$ mice. Because *Entpd7* is highly expressed in ECs of the small intestine, we established intestinal EC lines from wild-type and *Entpd7*$^{-/-}$ mice using transgenic mice harboring a temperature-sensitive mutation of the SV40 large tumor Ag gene under the control of an IFN-γ–inducible H-2K^{b} promoter element to analyze ATP levels in the ECs (26, 35, 36). ECs from wild-type and *Entpd7*$^{-/-}$ mice expressed keratin proteins equally as well as *Krt7* mRNA, indicating that these cells are ECs (Supplemental Fig. 3). *Entpd7* was highly expressed in wild-type ECs but not in *Entpd7*$^{-/-}$ ECs (Supplemental Fig. 3). Intracellular ATP levels were not altered between wild-type and *Entpd7*$^{-/-}$ ECs (Fig. 2B). Fecal concentrations of ATP were not different in *Entpd7*$^{-/-}$ mice compared with wild-type mice (Fig. 2C). However, ATP levels in the luminal contents of the small intestine were substantially increased in *Entpd7*$^{-/-}$ mice (Fig. 2D). We then created a ligated intestinal loop model to analyze alterations in luminal ATP levels. The proximal regions of the small intestine were ligated to make a loop in wild-type and *Entpd7*$^{-/-}$ mice. Then, ATP or PBS was injected into the

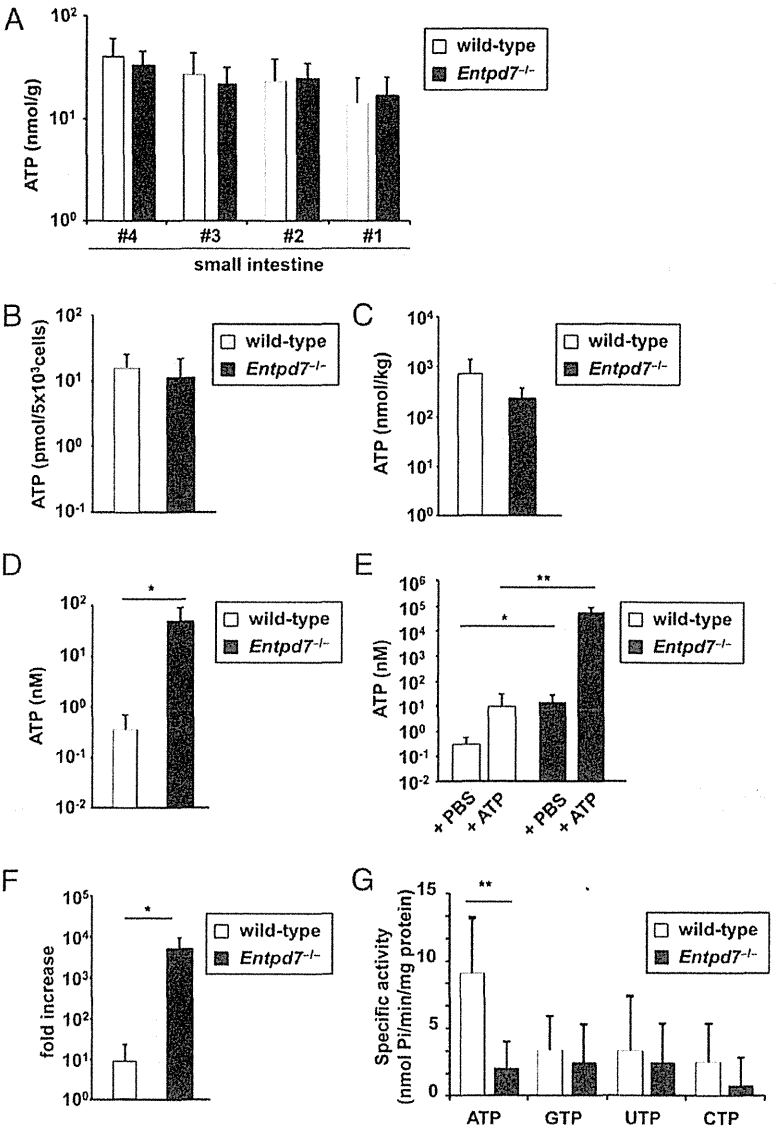

FIGURE 2. Increased luminal ATP levels in the small intestine of *Entpd7*$^{-/-}$ mice. (**A**) The small intestines of wild-type and *Entpd7*$^{-/-}$ mice were cut into quarters transversely. Each piece was weighed and lysed to measure ATP using a luciferin-luciferase assay. The smaller number denotes the more proximal site of the intestine. Data are representative of two independent experiments; means + SD. (**B**) Small intestinal ECs from wild-type and *Entpd7*$^{-/-}$ mice were lysed and analyzed for ATP levels, as described in (A). Data are representative of three independent experiments; means + SD. (**C**) Feces of wild-type and *Entpd7*$^{-/-}$ mice were dissolved in PBS, and ATP levels of the supernatants were measured as described in (A). Data are representative of three independent experiments and represent mean + SD of five mice. (**D**) Wild-type and *Entpd7*$^{-/-}$ mice were anesthetized, peritoneal cavities were opened, and the small intestine was ligated at 1.5 and 4.5 cm distal from the Treitz ligament to make a closed intestinal loop. PBS (300 μl) was injected into the lumen of the small intestinal loop, and the luminal fluid was recovered soon after the injection. ATP levels in the fluid were measured. Data are representative of three independent experiments and represent mean + SD of four mice. (**E**) ATP solution (1.5 mM) or PBS was injected into the intestinal loop, and the luminal fluid was collected 15 min later. ATP levels in the fluids were measured. (**F**) The fold increase in luminal ATP levels after ATP injection in the small intestine of wild-type and *Entpd7*$^{-/-}$ mice. Data are representative of three independent experiments and represent mean + SD of four mice. (**G**) NTP hydrolyzing activity in membrane preparations of intestinal EC lines. Activity for each of the four nucleoside triphosphates was assayed with crude membrane preparations from small intestinal ECs from wild-type and *Entpd7*$^{-/-}$ mice. Data are representative of three independent experiments; means + SD. $^{*}p < 0.05$, $^{**}p < 0.01$.

loop, and ATP levels were analyzed in the luminal contents 15 min later. ATP injection increased luminal ATP levels in wild-type and *Entpd7*$^{-/-}$ mice (Fig. 2E). There was a 10-fold increase observed in ATP-treated wild-type mice. In contrast, the ATP level was increased by >1000-fold in the luminal contents of *Entpd7*$^{-/-}$ mice (Fig. 2F). Thus, *Entpd7*$^{-/-}$ mice show an increased level of luminal ATP, possibly resulting from a serious defect in ATP-clearance activity in the small intestinal lumen. We then measured NTP (ATP, GTP, UTP, and CTP) hydrolyzing activity in membrane preparations of ECs (Fig. 2G). ATP was hydrolyzed most efficiently by the EC membrane fraction of wild-type mice. In addition, the ATP-hydrolyzing activity was severely impaired in the EC membrane fraction of *Entpd7*$^{-/-}$ mice. Thus, small intestinal ECs, which highly express ENTPDase7, have the ability to hydrolyze ATP. These findings indicate that ENTPDase7 is required for the maintenance of ATP levels in the small intestinal lumen.

Increased number of Th17 cells in the small intestinal lamina propria in Entpd7$^{-/-}$ *mice*

A previous study showed that luminal ATP in the intestine mediates Th17 cell development (10). In addition, extracellular ATP was shown to induce Th17 cell development via the inhibition of regulatory T cell functions (15). Therefore, we analyzed the number of CD4^{+} T cells expressing IL-17, IFN-γ, IL-10, and Foxp3 in the lamina propria of the small and large intestines. The numbers of IL-17–, IFN-γ–, IL-10–, and Foxp3-expressing CD4^{+} T cells were not altered in the large intestinal lamina propria of *Entpd7*$^{-/-}$ mice (Fig. 3A, 3C). In contrast, the number of IL-17–producing CD4^{+} T cells in the small intestinal lamina propria was markedly increased in *Entpd7*$^{-/-}$ mice compared with wild-type mice, although the numbers of IFN-γ^{+}, IL-10^{+}, and Foxp3^{+} T cells were not affected (Fig. 3B, 3C). The number of IL-17–producing CD4^{+} T cells was not increased in other lymphoid organs, such as the spleen, MLNs, and Peyer's patches of *Entpd7*$^{-/-}$ mice (Supplemental Fig. 4). Thus, *Entpd7*$^{-/-}$ mice showed elevation of Th17 cells in the small intestinal lamina propria. Consistent with *Entpd7*-expression patterns in the small intestine, the level of luminal ATP was higher in the distal region than in the proximal region of the small intestine of wild-type mice (Fig. 3D); accordingly, the number of IL-17–producing CD4^{+} T cells was higher in the distal region (Fig. 3E).

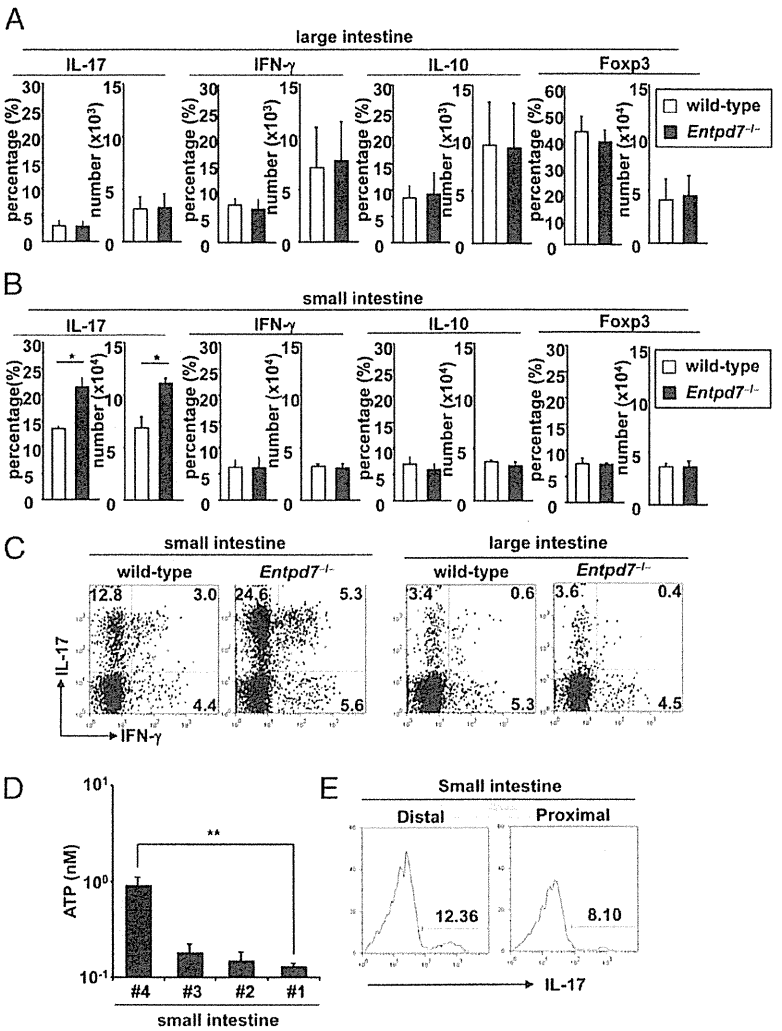

FIGURE 3. Enhanced Th17 cell development in the small intestine of *Entpd7*$^{-/-}$ mice. (**A** and **B**) The lamina propria lymphocytes were isolated from wild-type and *Entpd7*$^{-/-}$ mice, stimulated, permeabilized, stained for IL-17/IFN-γ/IL-10, and analyzed by flow cytometry. Percentages and total numbers of IL-17–, IFN-γ–, and IL-10–producing, as well as Foxp^{+} CD4^{+}, cells in the large intestinal (A) and the small intestinal (B) lamina propria. Data are mean + SD of four mice. (**C**) Representative FACS dot plots gated on intestinal lamina propria CD4^{+} cells of wild-type and *Entpd7*$^{-/-}$ mice. (**D**) The level of luminal ATP in the small intestine. The smaller number denotes the more proximal site of the intestine. ATP levels in the luminal fluid in the indicated portions of the small intestine were measured. Data are representative of three independent experiments and represent mean + SD of four mice. (**E**) The numbers of IL-17–producing CD4^{+} cells in the small intestine. The small intestinal lamina propria lymphocytes were isolated from proximal and distal portions of small intestine of wild-type mice and analyzed for production of IL-17 from CD4^{+} T cells by flow cytometry. Representative FACS dot plots gated on small intestinal lamina propria CD4^{+} cells. $^{*}p < 0.05$, $^{**}p < 0.01$.

Commensal microbiota-dependent, ATP-dependent increase in Th17 cells in Entpd7$^{-/-}$ *mice*

We analyzed whether increased Th17 cell development in the small intestine was intrinsic to the T cell itself or caused by extrinsic environmental factors. We first induced in vitro differentiation of splenic naive CD4^{+} T cells into Th17 cells. Naive CD4^{+} T cells were cultured in Th17 cell–skewing conditions and analyzed for IL-17 production (Fig. 4A). In vitro–differentiated CD4^{+} T cells from wild-type and *Entpd7*$^{-/-}$ mice produced almost equal amounts of IL-17, indicating that *Entpd7*$^{-/-}$ T cells were not intrinsically programmed to preferentially differentiate into Th17 cells. We then treated *Entpd7*$^{-/-}$ mice orally with combinations of four antibiotics (i.e., vancomycin, streptomycin, metronidazole, and ampicillin) from birth (Fig. 4B). In antibiotic-treated wild-type and *Entpd7*$^{-/-}$ mice, the number of IL-17–producing T cells, as well as IFN-γ– and IL-10–producing T cells, in the small intestinal lamina propria was dramatically reduced. These findings indicate that the augmentation of Th17 cells in *Entpd7*$^{-/-}$ mice was caused by altered environmental factors influenced by commensal microbiota. Recent data demonstrate that a specific microbiota, such as SFB, induces Th17 cell differentiation in the small intestine (37, 38). Therefore, we analyzed the number of intestinal bacteria in the luminal contents and epithelial layers of the small intestine of wild-type and *Entpd7*$^{-/-}$ mice (Fig. 4C). The number of intestinal bacteria was not altered in *Entpd7*$^{-/-}$ mice, indicating that *Entpd7* deficiency did not cause alteration of microbiota.

Because commensal microbiota were shown to influence luminal ATP level (10), we analyzed the effect of the blockade of ATP action. oATP, which antagonizes P2X receptors, was shown to be effective in modulating T cell responses in mice, especially Th17 cell responses (15). Therefore, *Entpd7*$^{-/-}$ mice were treated with oATP; however, the total number of CD4^{+} cells in the small intestinal lamina propria was not altered (Fig. 5A). In accordance with the previous finding that oATP inhibits T cell responses, such as cytokine production (14), the number of IFN-γ^{+} and IL-10^{+} CD4^{+} T cells was moderately reduced (Fig. 5B). Notably, the number of IL-17–producing CD4^{+} T cells was severely reduced in oATP-treated *Entpd7*$^{-/-}$ mice (Fig. 5C, 5D). In an intestinal inflammation model of immunocompromised *Cd3e*$^{-/-}$ mice transferred with conventional T cells, oATP treatment increased the number of Foxp3^{+} CD4^{+} T cells in MLNs of the diseased mice (14). However, *Entpd7*$^{-/-}$ mice treated with oATP did not show any increase in the number of Foxp3^{+} T cells in MLNs or the small intestinal lamina propria (Fig. 5E). Thus, the ATP antagonist severely decreased Th17 cells and moderately reduced IFN-γ– and IL-10–producing T cells. These findings indicate that the increased ATP level is responsible for enhanced Th17 cell development in the small intestine of *Entpd7*$^{-/-}$ mice.

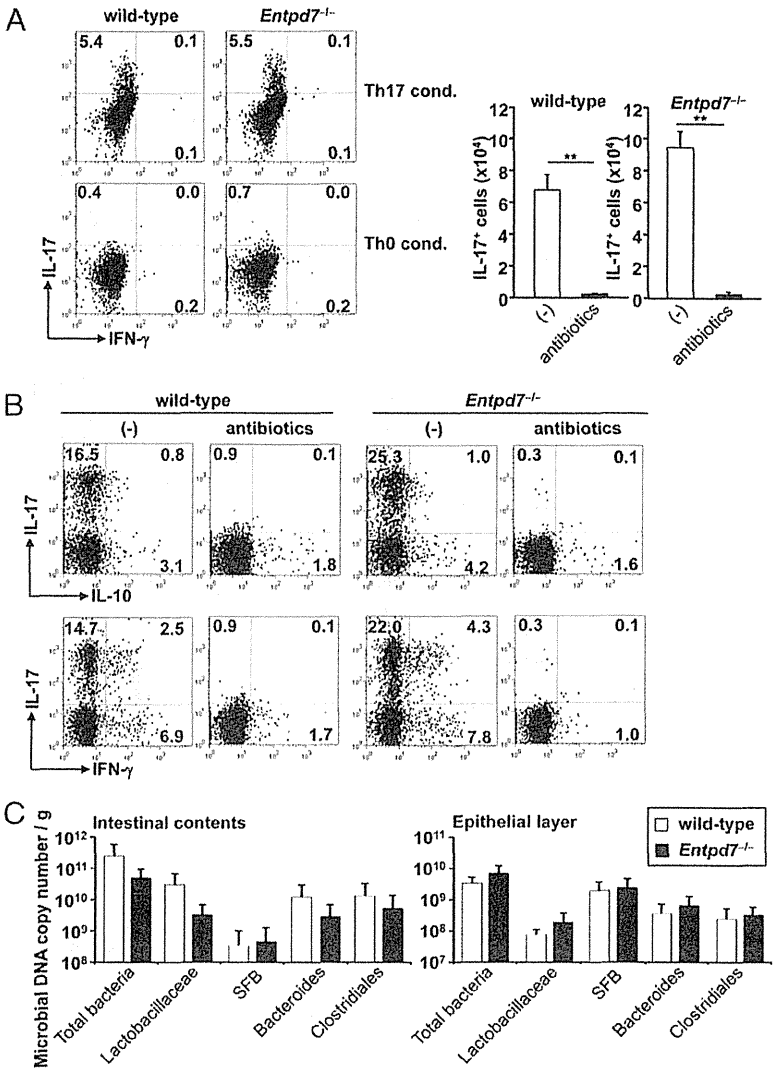

FIGURE 4. Decreased number of Th17 cells in antibiotic-treated *Entpd7*$^{-/-}$ mice. (**A**) Splenic naive CD4$^+$ T lymphocytes were cultured for 4 d under Th17-polarizing conditions (TGF-β, IL-6, anti–IFN-γ, and anti–IL-4) or Th0 conditions (anti–IFN-γ and anti–IL-4). Then, lymphocytes were harvested, stimulated, permeabilized, stained for IL-17 and IFN-γ, and analyzed by flow cytometry. Data are representative of three independent experiments. (**B**) Wild-type (n = 4) and *Entpd7*$^{-/-}$ (n = 4) mice were administered vancomycin, metronidazole, ampicillin, and neomycin sulfate in drinking water from birth. The small intestinal lamina propria lymphocytes were isolated at 8 wk of age and analyzed for production of IL-17, IFN-γ, and IL-10 from CD4$^+$ T cells by flow cytometry. Representative FACS dot plots and total numbers of cells gated on small intestinal lamina propria CD4$^+$ cells are shown. (**C**) Intestinal bacteria in the luminal contents and epithelial layers of the small intestines of wild-type and *Entpd7*$^{-/-}$ mice. DNA isolated from the luminal contents and epithelial layers of the small intestines was analyzed by real-time quantitative PCR using primers for bacterial group–specific 16S rRNA genes. Data are representative of two independent experiments and are mean + SD of five mice.

Resistance to intestinal C. rodentium *infection in Entpd7*$^{-/-}$ *mice*

A previous study showed that development of Th17 cells in the small intestine provides the resistance to oral infection with *C. rodentium* (38). Therefore, we orally infected wild-type and *Entpd7*$^{-/-}$ mice with *C. rodentium*. The CFU titers of bacteria in the spleen were measured at day 14 after the infection (Fig. 6A, 6B). The number of spleens that was invaded with *C. rodentium* was dramatically decreased in *Entpd7*$^{-/-}$ mice. Accordingly, *Entpd7*$^{-/-}$ mice had decreased numbers of *C. rodentium* in the spleen compared with wild-type mice. In addition, although some wild-type mice died after the oral *C. rodentium* infection, none of the *Entpd7*$^{-/-}$ mice died (Fig. 6C). Thus, *Entpd7*$^{-/-}$ mice are resistant to the intestinal bacterium *C. rodentium*.

Deteriorated EAE in Entpd7$^{-/-}$ *mice*

Enhanced Th17 responses are implicated in the development of several immune disorders, including EAE (39). Th17 cells, which develop in the small intestine, were also shown to induce inflammation in extraintestinal tissues, such as arthritis in the ankle joints (40). Furthermore, commensal microbiota were shown to be involved in the pathogenesis of EAE (41). Therefore, we used a MOG peptide–induced model of EAE in *Entpd7*$^{-/-}$ mice to determine the effect of ENTPDase7-mediated regulation of intestinal Th17 cells in inflammatory conditions in vivo. As shown in Fig. 7A, s.c. immunization of wild-type mice with the MOG peptide, together with pertussis toxin, induced encephalomyelitis associated with rapidly ascending paralysis appearing at approximately day 10–12. MOG peptide–immunized *Entpd7*$^{-/-}$ mice showed more severe clinical symptoms. We then analyzed cytokine production from CD4$^+$ T cells infiltrated into the CNS of the diseased mice (Fig. 7B). In wild-type and *Entpd7*$^{-/-}$ mice, infiltration of IL-17– and IFN-γ–producing CD4$^+$ T cells, as well as IL-17/IFN-γ double-producing cells, was observed. IL-17/IFN-γ double-producing CD4$^+$ cells increased markedly in *Entpd7*$^{-/-}$ mice compared with diseased wild-type mice. Thus, in the absence of *Entpd7*, severe EAE developed that was accompanied by an increased infiltration of CD4$^+$ T cells producing both IL-17 and IFN-γ.

Discussion

In the current study, we analyzed the physiological function of ENTPDase7, which is preferentially expressed in ECs of the small intestine. ENTPDase7 deficiency in mice led to increased ATP levels in the small intestinal lumen, indicating that ENTPDase7 is responsible for the maintenance of luminal ATP levels. The number of IL-17–producing Th17 cells in the small intestinal lamina propria was increased in *Entpd7*$^{-/-}$ mice. The number of Th17

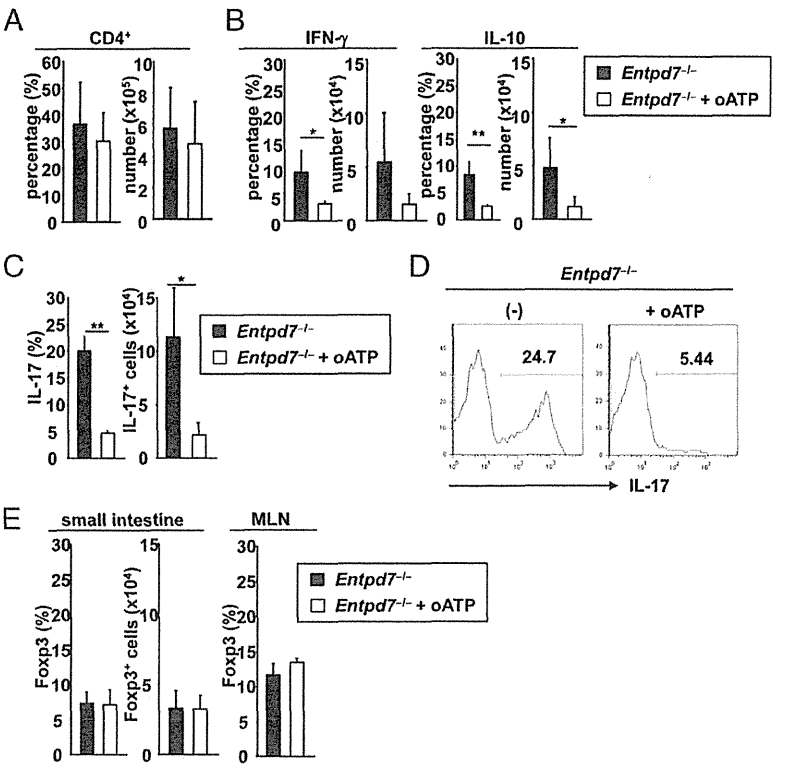

FIGURE 5. Decreased number of Th17 cells in oATP-treated *Entpd7*$^{-/-}$ mice. (**A–C**) *Entpd7*$^{-/-}$ mice were administered 100 μl of 6 mM oATP or PBS i.v. daily for 2 wk. The small intestinal lamina propria lymphocytes were then isolated and analyzed for production of IFN-γ, IL-10, and IL-17 from CD4$^+$ T cells by flow cytometry. The percentages and total numbers of CD4$^+$ T cells (A), IFN-γ and IL-10–producing CD4$^+$ T cells (B), and IL-17–producing CD4$^+$ T cells (C) in the small intestinal lamina propria of PBS- or oATP-treated *Entpd7*$^{-/-}$ mice. Data are representative of two independent experiments and are mean + SD of four mice. (**D**) Representative FACS graph showing IL-17 production gated on small intestinal lamina propria CD4$^+$ T cells of the indicated mice. (**E**) The percentages and total numbers of Foxp3$^+$ CD4$^+$ T cells in the small intestinal lamina propria and MLNs of PBS- or oATP-treated *Entpd7*$^{-/-}$ mice. Data are representative of two independent experiments and are mean + SD of three mice. $*p < 0.05$, $**p < 0.01$.

cells was decreased in *Entpd7*$^{-/-}$ mice in the absence of commensal microbiota or after ATP antagonist treatment. *Entpd7*$^{-/-}$ mice were resistant to infection with *C. rodentium*, against which Th17-related cytokines play a major role.

A previous report indicated that human ENTPDase7 is expressed in the membrane of intracellular compartments (28). The intracellular ATP level, which was analyzed using total-cell lysates, was not altered in *Entpd7*$^{-/-}$ ECs. However, given that the ATP concentration in the cytoplasm is >1 mM, whereas the ATP concentration in the extracellular compartment is usually <10 nM, ATP levels within the ENTPDase7-expressing cellular vesicles of ECs would be increased in the absence of ENTPDase7. Indeed, the membrane fraction of intestinal ECs had an enzymatic activity to hydrolyze ATP, and its activity was decreased in the absence of *Entpd7*. Because Entpd7 was highly expressed in goblet cells, as well as absorptive ECs, it is possible that *Entpd7* is

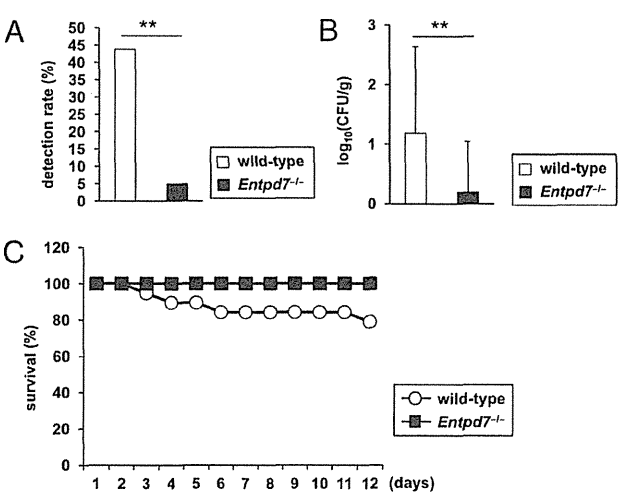

FIGURE 6. Resistance to intestinal *C. rodentium* infection in *Entpd7*$^{-/-}$ mice. (**A–C**) Wild-type (n = 19) and *Entpd7*$^{-/-}$ (n = 19) mice were infected orally with *C. rodentium*. (A) Detection rate of *C. rodentium* in the spleen on day 14. The pooled data of two independent experiments are shown. (B) Log_{10} CFU of *C. rodentium* in spleens. (C) Survival rate of the mice at the indicated time points. The pooled data of two independent experiments are shown. $**p < 0.01$.

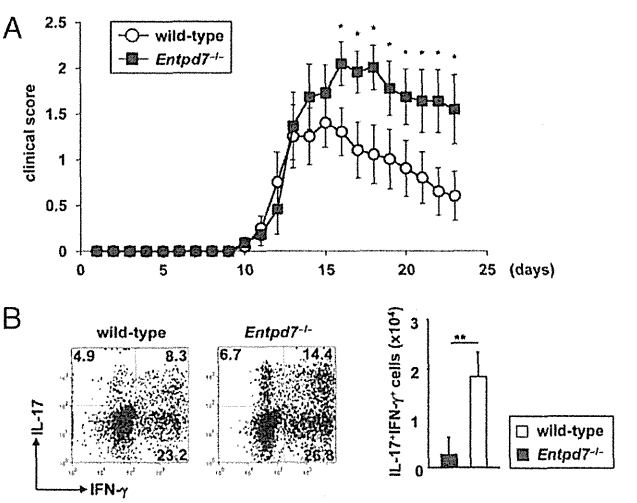

FIGURE 7. Severe EAE in *Entpd7*$^{-/-}$ mice. (**A**) Wild-type (n = 10) and *Entpd7*$^{-/-}$ (n = 11) mice were immunized with 100 μg MOG_{35-55} peptide in CFA; 100 ng of pertussis toxin was injected i.p. on days 0 and 2. The mean clinical score was calculated by averaging the scores of the mice in each group. Data are mean ± SEM at each time point. Experiments were performed twice with similar results. $*p < 0.05$. (**B**) Representative FACS dot plots gated on CD4$^+$ cells of the CNS in the indicated mice at day 17 after EAE induction (*left* and *middle panels*). CNS lymphocytes were isolated from wild-type and *Entpd7*$^{-/-}$ mice 17 d after EAE induction and analyzed for the production of IFN-γ and IL-17 from CD4$^+$ T cells by flow cytometry (*right panel*). Data are representative of five mice analyzed. $**p < 0.05$.

expressed in the membrane of mucin-containing vacuoles of goblet cells to control ATP levels in the vacuole. Given that goblet cells of the airway were shown to secrete ATP, as well as mucin (42), intestinal goblet cells might be a major source of luminal ATP, the level of which is closely regulated by ENTPDase7.

Human ENTPDase7 was shown to preferentially hydrolyze UTP, GTP, and CTP rather than ATP (28). However, the membrane fraction of mouse intestinal ECs effectively hydrolyzed ATP, and its activity was impaired by *Entpd7* deficiency. Thus, mouse ENTPDase7, unlike human ENTPDase7, effectively hydrolyzes ATP. Indeed, apparent differences in amino acid sequences are observed in a domain between the second and third apyrase-conserved regions, supporting that mouse and human ENTPDase7 have different substrate affinities.

Luminal ATP is supposed to be derived from ECs, as discussed above. In addition, commensal microbiota are a source of luminal ATP (10). In this regard, commensal microbiota, especially SFB, mediate Th17 cell development in the small intestine, possibly through ATP-independent mechanisms (37, 43). Therefore, in the small intestine, luminal ATP may mediate Th17 cell development cooperatively with Th17-inducing commensal microbiota. There is controversy as to how luminal ATP is sensed and induces Th17 development. Intestinal CX_3CR1^+ DCs were shown to extrude their dendrites into the lumen to sample intestinal Ags (44, 45). These intestinal DCs might sense luminal ATP via purinergic receptors. Alternatively, as reported in several studies, ECs sense extracellular ATP (11, 25, 46). Therefore, intestinal ECs trigger inflammatory responses to activate T cell development via ATP sensing. Indeed, intestinal ECs were shown to control DC functions (47).

C. rodentium is an enteric bacterium that colonizes the intestine of mice postinfection. Clearance of *C. rodentium* is shown to be dependent on Th17-related cytokines, such as IL-17 and IL-22 (48, 49). Data showing that mice lacking IL-23, a critical cytokine for Th17 cell development, are highly susceptible to *C. rodentium* infection also indicate that Th17-related cytokines are critical for the resistance to intestinal *C. rodentium* infection (50). Consistent with these facts, $Entpd7^{-/-}$ mice showing an increased number of Th17 cells in the small intestine are highly resistant to intestinal infection with *C. rodentium*. IL-22 and IL-17, which induce production of antibacterial peptides (REGIIIγ and β-defensins) from intestinal ECs (48, 51), are produced from other cell populations, such as innate lymphoid cells and γδT cells (52, 53). Therefore, Th17 cells, together with an innate type of IL-17–producing cells, contribute to intestinal pathogens.

In an EAE model, $CD4^+$ T cells producing both IL-17 and IFN-γ are observed in the CNS (54–56). It is still controversial whether these IL-17/IFN-γ double-producing T cells are Th1 or Th17 cells, but they do contribute to EAE pathogenesis (54). A study using $Il23ra^{-/-}$ mice, which showed a reduced number of Th17 cells, as well as IL-17/IFN-γ double-producing T cells and a normal number of Th1 cells, suggested that IL-17/IFN-γ double-producing T cells are derived from Th17 cells (57). Therefore, increased numbers of IL-17/IFN-γ double-producing T cells in the CNS of $Entpd7^{-/-}$ mice with EAE might be due to enhanced Th17 responses.

It remains unclear how Th17 cells residing in the small intestine mediate EAE. However, several lines of evidence indicate the relevance between gut immune cells and immune disorders in extraintestinal tissues: Th17 cells induced by SFB in the small intestinal lamina propria were shown to be responsible for the induction of autoimmune arthritis (40); alteration of the commensal flora composition influences the severity of EAE (41); and SFB-induced Th17 cells in the small intestine induce EAE (58). Thus, intestinal effector T cells are responsible for the induction of immune disorders in nongut tissues, including the CNS, and our present study demonstrates that enhanced intestinal Th17 responses can induce severe inflammatory conditions in these disease models.

In this study, we showed that an ENTPDase expressed by intestinal ECs regulates luminal ATP levels and, thereby, controls intestinal immune responses. Another ENTPDase, ENTPDase8, is selectively expressed by the ECs in the large intestine, as well as the small intestine (T. Kusu and K. Takeda, unpublished observations). Characterization of ENTPDase8 functions in terms of regulation of intestinal immune responses will be an interesting issue to be addressed in the future.

Acknowledgments

We thank C. Hidaka for secretarial assistance and Y. Magota for technical assistance.

Disclosures

The authors have no financial conflicts of interest.

References

1. Burnstock, G. 2007. Physiology and pathophysiology of purinergic neurotransmission. *Physiol. Rev.* 87: 659–797.
2. Vassort, G. 2001. Adenosine 5′-triphosphate: a P2-purinergic agonist in the myocardium. *Physiol. Rev.* 81: 767–806.
3. Junger, W. G. 2011. Immune cell regulation by autocrine purinergic signalling. *Nat. Rev. Immunol.* 11: 201–212.
4. Piccini, A., S. Carta, S. Tassi, D. Lasiglié, G. Fossati, and A. Rubartelli. 2008. ATP is released by monocytes stimulated with pathogen-sensing receptor ligands and induces IL-1beta and IL-18 secretion in an autocrine way. *Proc. Natl. Acad. Sci. USA* 105: 8067–8072.
5. Yu, H. B., and B. B. Finlay. 2008. The caspase-1 inflammasome: a pilot of innate immune responses. *Cell Host Microbe* 4: 198–208.
6. Chen, Y., R. Corriden, Y. Inoue, L. Yip, N. Hashiguchi, A. Zinkernagel, V. Nizet, P. A. Insel, and W. G. Junger. 2006. ATP release guides neutrophil chemotaxis via P2Y2 and A3 receptors. *Science* 314: 1792–1795.
7. Elliott, M. R., F. B. Chekeni, P. C. Trampont, E. R. Lazarowski, A. Kadl, S. F. Walk, D. Park, R. I. Woodson, M. Ostankovich, P. Sharma, et al. 2009. Nucleotides released by apoptotic cells act as a find-me signal to promote phagocytic clearance. *Nature* 461: 282–286.
8. Kronlage, M., J. Song, L. Sorokin, K. Isfort, T. Schwerdtle, J. Leipziger, B. Robaye, P. B. Conley, H. C. Kim, S. Sargin, et al. 2010. Autocrine purinergic receptor signaling is essential for macrophage chemotaxis. *Sci. Signal.* 3: ra55.
9. Trautmann, A. 2009. Extracellular ATP in the immune system: more than just a "danger signal". *Sci. Signal.* 2: pe6.
10. Atarashi, K., J. Nishimura, T. Shima, Y. Umesaki, M. Yamamoto, M. Onoue, H. Yagita, N. Ishii, R. Evans, K. Honda, and K. Takeda. 2008. ATP drives lamina propria T(H)17 cell differentiation. *Nature* 455: 808–812.
11. Weissmüller, T., E. L. Campbell, P. Rosenberger, M. Scully, P. L. Beck, G. T. Furuta, and S. P. Colgan. 2008. PMNs facilitate translocation of platelets across human and mouse epithelium and together alter fluid homeostasis via epithelial cell-expressed ecto-NTPDases. *J. Clin. Invest.* 118: 3682–3692.
12. Ivison, S. M., M. E. Himmel, M. Mayer, Y. Yao, A. Kifayet, M. K. Levings, and T. S. Steiner. 2011. The stress signal extracellular ATP modulates antiflagellin immune responses in intestinal epithelial cells. *Inflamm. Bowel Dis.* 17: 319–333.
13. Heiss, K., N. Jänner, B. Mähnss, V. Schumacher, F. Koch-Nolte, F. Haag, and H. W. Mittrücker. 2008. High sensitivity of intestinal CD8+ T cells to nucleotides indicates P2X7 as a regulator for intestinal T cell responses. *J. Immunol.* 181: 3861–3869.
14. Schenk, U., A. M. Westendorf, E. Radaelli, A. Casati, M. Ferro, M. Fumagalli, C. Verderio, J. Buer, E. Scanziani, and F. Grassi. 2008. Purinergic control of T cell activation by ATP released through pannexin-1 hemichannels. *Sci. Signal.* 1: ra6.
15. Schenk, U., M. Frascoli, M. Proietti, R. Geffers, E. Traggiai, J. Buer, C. Ricordi, A. M. Westendorf, and F. Grassi. 2011. ATP inhibits the generation and function of regulatory T cells through the activation of purinergic P2X receptors. *Sci. Signal.* 4: ra12.
16. Yegutkin, G. G. 2008. Nucleotide- and nucleoside-converting ectoenzymes: Important modulators of purinergic signalling cascade. *Biochim. Biophys. Acta* 1783: 673–694.
17. Schetinger, M. R., V. M. Morsch, C. D. Bonan, and A. T. Wyse. 2007. NTPDase and 5′-nucleotidase activities in physiological and disease conditions: new perspectives for human health. *Biofactors* 31: 77–98.
18. Robson, S. C., J. Sévigny, and H. Zimmermann. 2006. The E-NTPDase family of ectonucleotidases: Structure function relationships and pathophysiological significance. *Purinergic Signal.* 2: 409–430.
19. Maliszewski, C. R., G. J. Delespesse, M. A. Schoenborn, R. J. Armitage, W. C. Fanslow, T. Nakajima, E. Baker, G. R. Sutherland, K. Poindexter, C. Birks,